

## 14. SITE 745<sup>1</sup>

### Shipboard Scientific Party<sup>2</sup>

#### HOLE 745A

**Date occupied:** 8 February 1988  
**Date departed:** 9 February 1988  
**Time on hole:** 9 hr, 30 min  
**Position:** 59°35.71'S, 85°51.60'E  
**Bottom felt (rig floor; m; drill-pipe measurement):** 4093.0  
**Distance between rig floor and sea level (m):** 10.5  
**Water depth (drill-pipe measurement from sea level, m):** 4082.5  
**Total depth (rig floor; m):** 4103.5  
**Penetration (m):** 10.5  
**Number of cores (including cores with no recovery):** 1  
**Total length of cored section (m):** 10.0  
**Total core recovered (m):** 9.86  
**Core recovery (%):** 98  
**Oldest sediment cored:**  
Depth sub-bottom (m): 10.5  
Nature: diatom ooze  
Earliest age: Quaternary  
Measured velocity (km/s): 1.489

#### HOLE 745B

**Date occupied:** 9 February 1988  
**Date departed:** 10 February 1988  
**Time on hole:** 1 day, 20 hr, 45 min  
**Position:** 59°35.71'S, 85°51.60'E  
**Bottom felt (rig floor; m; drill-pipe measurement):** 4093.0  
**Distance between rig floor and sea level (m):** 10.5  
**Water depth (drill-pipe measurement from sea level, m):** 4082.5  
**Total depth (rig floor; m):** 4308.0  
**Penetration (m):** 215.0  
**Number of cores (including cores with no recovery):** 241  
**Total length of cored section (m):** 215.0  
**Total core recovered (m):** 220.72  
**Core recovery (%):** 102  
**Oldest sediment cored:**  
Depth sub-bottom (m): 215.0  
Nature: clayey diatom ooze and diatomaceous clay  
Earliest age: late Miocene  
Measured velocity (km/s): 1.537  
**Principal results:** Site 745 (59°35.71'S, 85°51.60'E; water depth 4082.5 m; target Site SKP-8A) was drilled near the completion of

Ocean Drilling Program (ODP) Leg 119 after the drilling objectives on the Kerguelen Plateau and in Prydz Bay had been accomplished. The departure of the support vessel *Maersk Master* and the presence of persistent icebergs prevented drilling at more southerly sites. Site 745 was chosen to provide a deep-water Neogene reference section that could be compared with sections at shallow to intermediate water depths obtained at Sites 736 through 738 and 744 (631–2317.8 m). The site is situated on a large sediment drift at the base of the southeastern slope of the southern Kerguelen Plateau.

A 215-m-thick section of uppermost Miocene through Quaternary silty diatom ooze and diatom clay was cored in two holes at Site 745. One lithologic unit consisting of two subunits is recognized. Subunit IA, from 0 to 37 m below seafloor (mbsf), is dominated by a diatom ooze (with 70%–90% diatoms), with some minor amounts of quartz-feldspar silt, radiolarians, or clay. Subunit IB is characterized by more clearly alternating diatom ooze and diatomaceous clay intervals on a scale of decimeters to a few meters, of which the clay-rich horizons contain < 50% diatoms; the silt content in this subunit is also significant. Minor claystone, silt, and volcanic ash layers also occur. Scattered granules and small pebbles are disseminated throughout much of the core.

The succession is mixed pelagic-terrigenous. The pelagic component is due to production in the upper part of the water column. The terrigenous quartz-silt component, along with the granules and pebbles, is derived from a metamorphic terrain, and some clasts resemble the gneisses found in the Prydz Bay diamictites. They are considered to have been transported to the site by ice rafting. The ice-rafted component is greatest in lower Pliocene and Quaternary sediments, but is never entirely absent in any part of the sequence. The variation in the content of the fine-grained terrigenous component may reflect variation in bottom-current activity or variations in the supply of clay to the deep sea, possibly controlled by changing positions of the Antarctic ice sheet in relation to the shelf edge.

Diatoms and radiolarians are common and generally well preserved throughout the section whereas calcareous microfossils are sparse and sporadic. Southern Ocean diatom and radiolarian zonations are readily applicable, and a good magnetostratigraphy identifies the Brunhes, Matuyama, Gauss, and Gilbert polarity chrons as well as the upper normal event of Chron C3A. As at Sites 737, 738, and 744, the uppermost Miocene (6.1–5.1 Ma) contains warm-water diatoms of the genera *Nitzschia* and *Thalassiosira*.

Within the Quaternary and upper Pliocene, cycles of more terrigenous-rich sediment alternating with more diatom-rich sediment are common. The diatom *Eucampia antarctica* has been shown to be more abundant in South Atlantic sediment within upper Quaternary intervals containing increased ice-rafted detritus. This diatom appears to be more abundant in the terrigenous-rich intervals at Site 745, implying that these cycles may be caused by glacial-interglacial oscillations.

#### BACKGROUND AND OBJECTIVES

Site 745 (target Site SKP-8A) was drilled near the end of ODP Leg 119 after the primary Kerguelen Plateau and Prydz Bay programs had been completed. The site is located in deep water (4082.5 m) under the influence of modern day Antarctic Bottom Water, and, thus, it contrasts with the intermediate water depths of Sites 738 and 744 (2263 and 2307 m, respectively) and the relatively shallow depths of Sites 736 and 737 (639 and 564 m, respectively). Additional Kerguelen Plateau sites planned for drilling on Leg 120 lie in intermediate water depths ranging from 1160 to 1700 m, so occupation of Site 745 adds a deep-wa-

<sup>1</sup> Barron, J., Larsen, B., et al., 1989. *Proc. ODP, Init. Repts.*, 119: College Station, TX (Ocean Drilling Program).

<sup>2</sup> Shipboard Scientific Party is as given in the list of Participants preceding the contents.

ter site to the paleoceanographic transect of Legs 119 and 120. Determination of the effects of Antarctic Bottom Water on sediment composition (carbonate vs. noncarbonate), on depositional history (continuous deposition vs. hiatuses), and on the microflora and microfauna (diatom and radiolarian assemblages) at Site 745 will be especially important in documenting the Oligocene and Neogene paleoceanographic history of the southern Indian Ocean.

Target Site SKP-8 (61°17'S, 86°46'E) was the preferred deep-water site selected by JOIDES panels. However, heavy iceberg concentration at that latitude combined with the departure of the ice-support vessel *Maersk Master*, caused the program to be shifted farther north to target Site SKP-8A, which lies about 200 km northwest of SKP-8.

Site 745 is on a sediment ridge along the southeast slope of the Kerguelen Plateau. The ridge shows characteristics of being a sediment drift on seismic lines. An objective at Site 745 was to determine the source of detrital sediment if it made up a significant percentage of the sediments there. If the sediment sequence at Site 745 is a sediment drift, it may have been derived from downslope movement off the Kerguelen Plateau, from northward transport of sediment displaced down the Antarctic continental slope, or a combination of the two. In addition, Site 745 should contain a good Oligocene to Neogene ice-rafting record, and comparison of that record with that of the other Kerguelen Plateau sites as well as the Prydz Bay sites should be possible.

## SITE GEOPHYSICS

### Site Survey

A survey line (ODP line 119-10) was recorded on the approach to Site 745 using the standard geophysical gear (see "Explanatory Notes" chapter, this volume) and Transit satellite navigation (Fig. 1). Global Positioning System satellite navigation was not available. Seas were calm during the survey and only one iceberg was within 16 km of the site. The survey line began on the upper flank of Kerguelen Plateau, and we planned to trace the sedimentary section into the abyssal basin (4500 m) where Site 745 was located. The first part of the seismic line was of low quality because only one water gun was operational and bathymetric relief was steep.

A tentative site was selected and the seismic line was continued for 1 hr to verify the site location. The ship was turned onto a reciprocal course, and sonobuoy 9 was deployed 13.5 km from the tentative site and recorded to an offset of 15 km. A beacon was dropped (shotpoint 3602) at the site. The seismic gear was recovered, and the ship returned to the site to begin drilling operations. The seismic results are discussed in "Seismic Stratigraphy" section (this chapter).

### Sonobuoy Data

Sonobuoy 9 was used to study the velocity structure of the sedimentary section underlying Site 745 and to determine a basement refraction velocity.

The sonobuoy was deployed successfully, but the hydrophone did not drop to more than 2–3 m below the surface because water-gurgling sounds occurred throughout the buoy. The high background water noise, the small seismic source (two 80-in.<sup>3</sup> water guns), and the very deep water (4082.5 m) resulted in a weak sonobuoy record (Fig. 2). Because of the deep water, the sonobuoy data were recorded with incremental deep-water delays to preserve the direct-wave arrival. Reflection arrivals only were recorded in the analog record, although refraction arrivals may be present and greatly suppressed by the high noise levels.

Five wide-angle reflections, including the seafloor and basement, could be traced to offsets of up to 10 km. However, the direct wave could only be seen clearly for offsets of several hun-

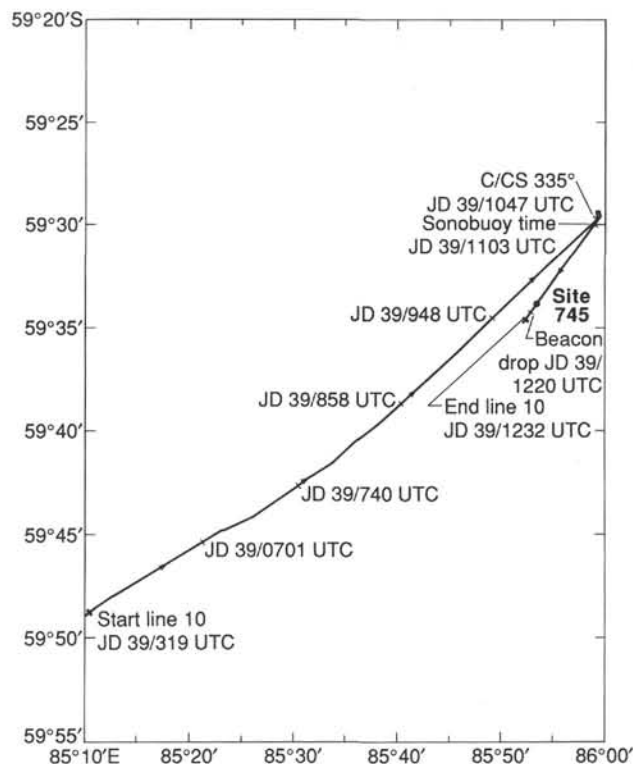


Figure 1. Index map of seismic lines recorded during site surveys for Site 745.

dred meters, beyond which the arrivals were very weak and uncertain. Minor corrections (–18 m/s) were added to rms and refraction velocities to correct for a questionable direct wave (see sonobuoy error discussion, "Underway Geophysics" chapter, this volume).

Although the sonobuoy record was poor, the wide-angle reflections could be traced continuously over a large distance, especially reflector CC (Fig. 3), which could be followed to the end of the sonobuoy at a 15-km offset. The rms velocity solutions for all reflections were good (e.g., nearly linear on distance-squared vs. time-squared plots; Table 1). Interval velocities could only be computed using four reflectors (AA, CC, DD, and EE). An interval velocity for layer AA–BB could not be computed because the smaller rms velocity for BB (caused by thickening of layer AA–BB, Fig. 4) did not allow a stable velocity computation in the large water depths.

Interval velocities for the sedimentary section range from 1.86 to 2.43 km/s. A refraction velocity for acoustic basement was not recorded. The prominent reflector at about 6.06 s in the seismic profile (Fig. 4) is the strongest wide-angle reflection in the sonobuoy data (CC, Fig. 3). A distinct velocity increase from 1.86 to 2.37 km/s occurs across this reflector. The great complexity of reflections and the abrupt velocity increase, both directly beneath reflector CC, indicate that a major lithologic change, and possible unconformity, occurs at this depth. An alternate explanation is that reflector CC is a diagenetic boundary with more highly indurated and cemented strata beneath CC. The depth to CC is about 475 mbsf, based on sonobuoy estimates.

The velocity of the well-layered strata directly above basement is 2.43 km/s, which is only slightly higher than the velocity of the overlying rocks. The total thickness of the sedimentary section, from reflectors AA to EE, is 1359 m.

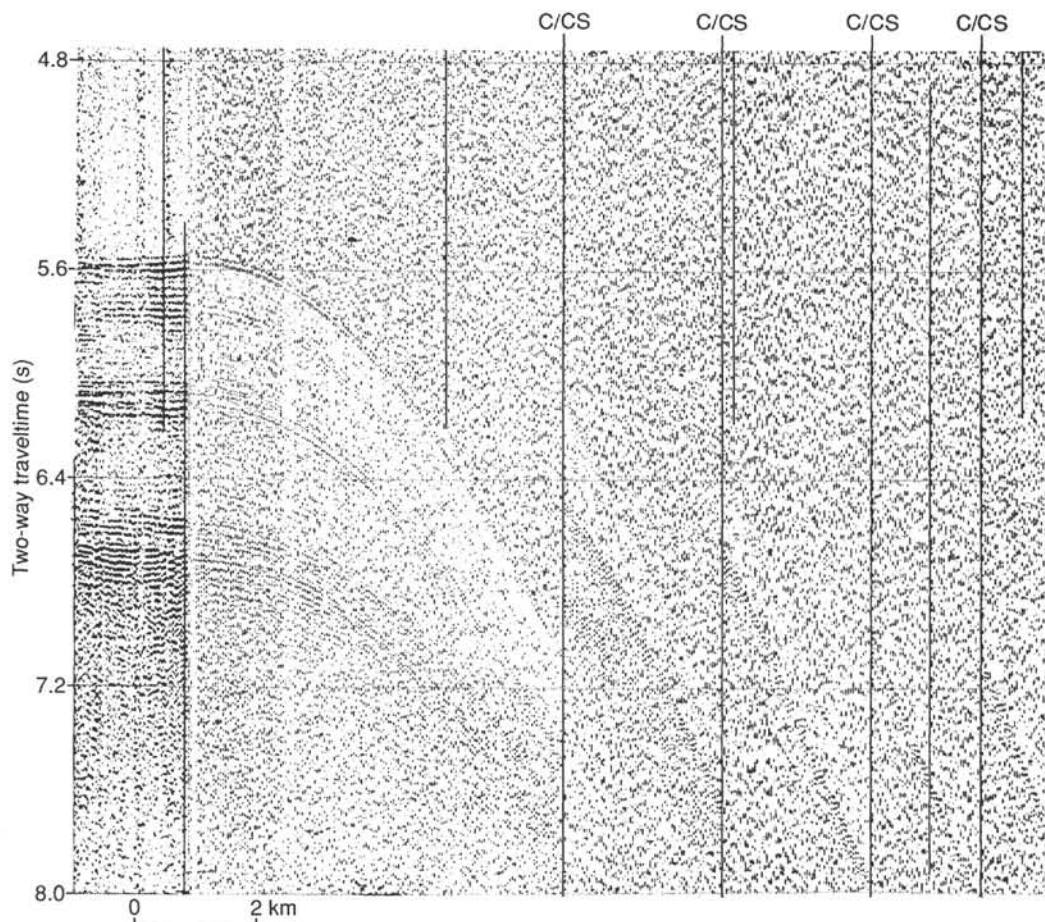


Figure 2. Vertical-incident seismic and sonobuoy seismic record for sonobuoy station 9. Site 745 lies about 13.5 km from where the sonobuoy was deployed. See Figure 1 for location; C/CS (change scale) indicates that the deep-water delay has been increased by 1 s.

## OPERATIONS

### Sites 744 to 745

The final drill site of the voyage had been revised to target Site SKP-8A from the previously planned SKP-8 because of the large amount of ice found at the latitude of SKP-8 on the transit to Site 744. ODP management gave clearance to drill the site, which had been surveyed and proposed previously but not scheduled for drilling. Site 745 is located about 306 km north-east of Site 744 at a latitude that was anticipated to be ice-free. Good weather permitted excellent transit speed, but the icebergs persisted. The vessel was forced to slow to half speed during the hours of darkness, when snow limited visibility further. A few icebergs were still visible when the site coordinates were crossed.

The profile was extended about a kilometer past that point before turning onto a reciprocal heading and deploying a sonobuoy for a refraction profile. The beacon was dropped about 9.7 km southwest of the originally-proposed site on the basis of the new seismic profile. The ship then continued to profile about 3.2 km past the drop point before returning to the beacon.

### Site 745—Kerguelen Sediment Ridge

#### Hole 745A

The pipe trip was slowed because the water depth was about 1300 m greater than the longest drill string previously deployed on the leg. The additional drill pipe had to be measured and

“rabbited.” Four joints of pipe were found to be restricted by rust scale and had to be laid out. The positioning beacon failed during the pipe trip and had to be replaced by a standby unit.

The site lay near the boundary between zones in the water velocity correction tables. The precision depth recorder (PDR) depth was 4095 m, with the adjacent zone reading 6 m deeper. The bit was positioned at 4093.5 m for the first advanced piston corer (APC) attempt. The core barrel was retrieved full, having been shot from below the seafloor. As the mud line was of scientific importance, the bit was repositioned 5 m higher and a second spud attempt was made.

#### Hole 745B

A new hole was designated because the same interval was cored twice. The second spud attempt recovered 5.5 m of sediment, indicating a seafloor depth of 4082.5 m.

APC cores were taken in soft diatom ooze to 128.5 mbsf with excellent recovery and core quality (Table 2). Because an iceberg moved toward the site, an 8.5-hr delay was needed while the pipe was tripped to just below seafloor and the iceberg’s progress plotted. After entering the warning zone, the iceberg changed course and slowly drifted back out of the area, permitting resumed operations in Hole 745B.

After only 10 additional cores, another iceberg was plotted coming in from the west, headed directly for the drill site at about 0.7 kt. Operations were again interrupted, and the new iceberg, which did not veer off, forced abandonment of the hole.

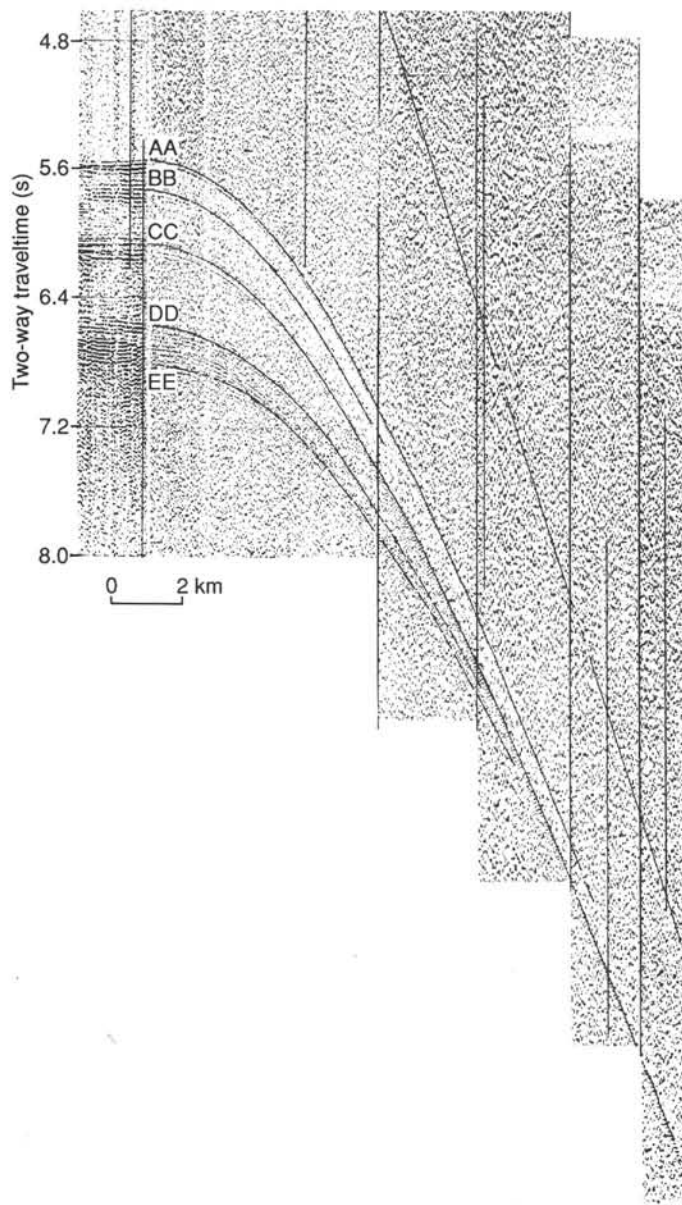


Figure 3. Vertical-incident seismic and sonobuoy seismic record for Site 745 showing wide-angle reflection interpretations. Letters denote layers given in Table 1; see Figure 1 for location.

## LITHOSTRATIGRAPHY AND SEDIMENTOLOGY

Site 745 was drilled in 4082.5 m of water with the intention of reaching about 400 mbsf. However, drilling was terminated at 215.0 mbsf when an approaching iceberg necessitated displacement to another site. The following site (746) was drilled with the intention of continuing the Site 745 succession downward. Core recovery was excellent at Site 745, achieving 103%, this figure possibly reflecting expansion of the core after extraction.

The sequence recovered consists almost entirely of diatom ooze and diatomaceous clay, spanning the interval from latest Miocene to Quaternary. A single unit with two subunits was defined, the boundary between them being placed somewhat arbitrarily at the top of a clay-rich layer at 50 cm in Section 119-745B-5H. Subunit IA (0–37 mbsf) is dominated by a diatom ooze (with 70%–90% diatoms), with some minor amounts of quartz-feldspar silt, radiolarians, or clay. Some diffuse horizons

Table 1. Preliminary results for Sonobuoy 9, Site 745.

Horizon <sup>a</sup>	Vrms (km/s)	Vint <sup>b</sup> (km/s)	Ti <sup>b</sup> (s)	Zi (km)
AA	1.490	1.86	5.55	4.083
<sup>c</sup> BB	1.410	—	5.73	—
CC	1.525	2.37	6.06	4.558
DD	1.605	2.43	6.56	5.150
EE	1.641	—	6.80	5.442

Note: Vrms = rms velocity for horizon; Vint = interval velocity computed using Vrms, Ti, and Dix equation (e.g., Vint between horizons AA and CC is 1.86 km/s); Ti = vertical-incidence reflection time (two-way) to horizon; Zi = total depth from sea level to horizon (water depth = 4082.5 m).

<sup>a</sup> Letters of horizons do not correlate between drill sites and do not correspond to prior stratigraphic analyses.

<sup>b</sup> Velocities and times used for computing depths Zi.

<sup>c</sup> Layer BB was not used for interval velocity computations.

with more clay also occur. Subunit IB (37–215.0 mbsf, total depth) is characterized by more clearly alternating diatom ooze and diatomaceous clay intervals on a scale of decimeters to a few meters, of which the clay-rich horizons contain <50% diatoms. The silt content in this subunit is also significant, reaching a maximum of 35%. Minor claystone, silt, and volcanic ash layers also were noted, all of which are only a few centimeters thick at most.

A significant feature of the site is the presence throughout most of the core of dispersed limestones, granules, and small pebbles originating from a metamorphic basement source area.

All percentages of biogenic and detrital material discussed in this chapter are based on smear slide analyses of about three per core. However, marked variations probably exist between sampling points, so this work gives only a generalized picture of compositional variations. High-resolution core sampling (at least every meter) was done to determine more precisely the nature of the changes. As at previous sites, discrimination between quartz and fresh untwinned feldspar grains proved difficult in smear slides. Therefore, these two minerals were considered in combination.

The lithostratigraphic and smear slide data are presented in the barrel sheets and are summarized in Figures 5 and 6.

The recovered succession is largely mixed pelagic and detrital. The pelagic component may have accumulated at depths similar to those of today and was occasionally subjected to bottom current activity. From the regional setting and seismic stratigraphy, such currents may have been strongly erosional at times, although obvious erosional surfaces in the core have not been seen. We believe the quartz-silt component, along with the granules and pebbles and possibly much of the clay, was transported to the site by ice rafting. The ice-rafted component is greatest in lower Pliocene and Quaternary sediments, but is never entirely absent in any part of the sequence. Transport of clay from submarine slopes may also be important. Reworked older diatoms and radiolarians occur throughout the sequence. Benthic diatoms and other diatoms associated with the shelf are also found, implying that some downslope movement off the Kerguelen Plateau probably occurred, either from the north, the west, or from Antarctica.

## Drilling Deformation

All coring was accomplished using APC coring techniques. Soupy disturbance characterizes the 1 m of sediment below the mud line in Hole 745A (Core 119-745A-1H). In Hole 745B the

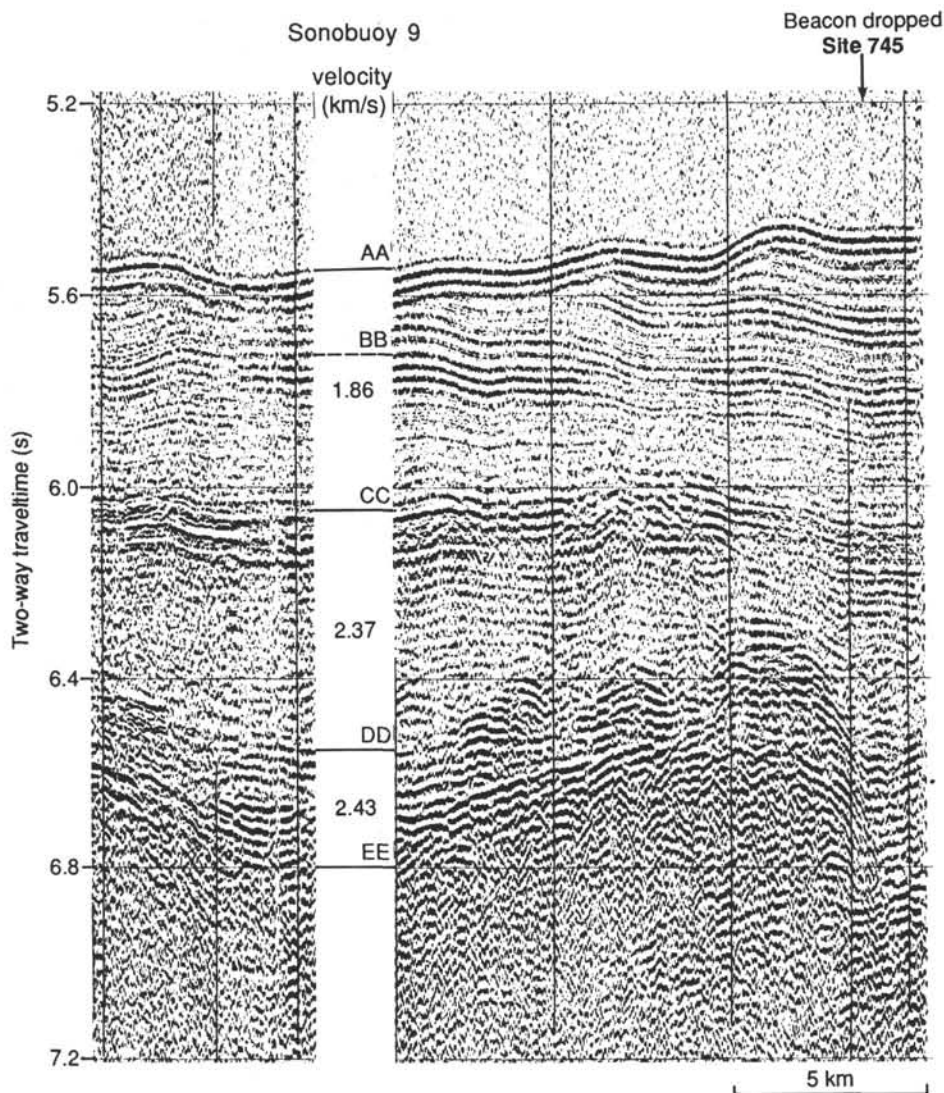


Figure 4. Vertical-incident seismic profile near Site 745 showing interval velocities computed from wide-angle reflections in sonobuoy 9.

mud line was recovered, and these uppermost sediments are better preserved than in Hole 745A. Short intervals of soupy disturbance also were seen at the top of Section 1 in Cores 119-745B-2H, 119-745B-3H, 119-745B-5H to 119-745B-8H, 119-745B-11H, 119-745B-17H, and 119-745B-20H to 119-745B-22H. In the deeper cores this part appears to be from downhole drilling contamination. Throughout the rest of the recovered core, deformation was limited to a bowing of laminae and, below Core 119-745B-8H, to fracturing in the more competent sediments.

### Lithostratigraphy

#### Unit I

Core 119-745A-1H and Core 119-745B-1H through Section 119-745B-24H; depth, 0–215 mbsf.  
Age: late Miocene to Quaternary.

The only unit defined in this core is made up almost entirely of diatom ooze and diatomaceous clay. Two subunits have been identified to provide a more detailed analysis.

#### Subunit IA

Core 119-745A-1H and Core 119-745B-1H through Section 119-745B-5H-3, 50 cm; depth, 0–37.0 mbsf.  
Age: Quaternary.

Subunit IA consists of diatom ooze, with minor silt at intervals throughout and minor radiolarians in Cores 119-745B-2H and 119-745B-3H. A wide variety of colors, dominated by greens, olives, and browns, is represented: greenish gray (unnamed—10GY 4/1 and 5G 5/1), dark greenish gray (5G 4/1 and 5G 3/1), grayish green (10GY 3/1 and 5G 5/1), dark gray (unnamed—10Y 5/1), dark gray (5Y 4/1), gray (5Y 5/1), light gray (unnamed—10Y 6/1 and 5GY 6/1), olive gray (5Y 4/2 and 5Y 5/2), light olive gray (5Y 6/2), pale olive (5Y 6/3), olive (5Y 5/3), brown (unnamed—2.5Y 5/3), pale brown (2.5Y 6/3 and 2.5Y 4/3), and grayish brown (2.5Y 5/2). The colors tend to become darker and more gray downcore.

Cores from 119-745B-2H downward are characterized by intervals with smoother and rougher textured cut surfaces separated by diffuse boundaries (Fig. 7). This may reflect more clay

Table 2. Coring summary, Site 745.

Core no.	Date (Feb. 1988)	Time	Depth (mbsf)	Length		Recovery (%)
				cored (m)	recovered (m)	
119-745A-						
1H	9	0325	0.5-10.5	10.0	9.86	98.6
				10.0	9.86	98.6
119-745B-						
1H	9	0430	0.0-5.0	5.0	5.09	102.0
2H	9	0530	5.0-14.5	9.5	9.79	103.0
3H	9	0640	14.5-24.0	9.5	9.45	99.5
4H	9	0745	24.0-33.5	9.5	9.79	103.0
5H	9	0845	33.5-43.0	9.5	9.83	103.0
6H	9	0955	43.0-52.5	9.5	9.33	98.2
7H	9	1055	52.5-62.0	9.5	9.76	103.0
8H	9	1200	62.0-71.5	9.5	9.85	103.0
9H	9	1250	71.5-81.0	9.5	10.03	105.6
10H	9	1410	81.0-90.5	9.5	9.86	104.0
11H	9	1630	90.5-100.0	9.5	9.79	103.0
12H	9	1730	100.0-109.5	9.5	10.02	105.5
13H	9	1830	109.5-119.0	9.5	9.98	105.0
14H	9	1930	119.0-128.5	9.5	9.94	104.0
15H	10	0520	128.5-138.0	9.5	9.05	95.2
16H	10	0615	138.0-139.0	1.0	0.02	2.0
17H	10	0710	139.0-148.5	9.5	9.72	102.0
18H	10	0800	148.5-158.0	9.5	9.92	104.0
19H	10	0900	158.0-167.5	9.5	10.01	105.3
20H	10	1000	167.5-177.0	9.5	9.89	104.0
21H	10	1225	177.0-186.5	9.5	10.03	105.6
22H	10	1320	186.5-196.0	9.5	9.54	100.0
23H	10	1420	196.0-205.5	9.5	9.97	105.0
24H	10	1525	205.5-215.0	9.5	10.06	105.9
				215.0	220.72	102.7

in the smooth zones, although smear slide data indicate that the differences are not marked.

The diatom ooze contains 70%–90% diatoms, 0%–15% radiolarians, 0%–15% clay, and 1%–24% quartz and feldspar silt. The clay and diatom components vary in inverse relationship with each other (Fig. 5). Minor components include traces of glass, amphiboles, and opaque and accessory minerals. The calcium carbonate content is low ( $<< 1\%$ ), as is the organic carbon (0.27%–0.42% from three samples) (see "Organic Chemistry" section, this chapter).

Parts of the sediment are affected by bioturbation. Elsewhere, darker mottling is well developed, which may also be a bioturbation feature. Several open burrows up to 1 cm in diameter occur in Cores 119-745B-1H and 119-745B-4H. The burrows are coated on the inside with a film of mud, and a few are surrounded by a greenish halo. A few smears of manganese oxide are present, possibly related to the burrows.

Throughout the subunit at irregular intervals, laminae from a few millimeters to centimeters in thickness separate more homogeneous intervals. Their colors vary from dark gray (5Y 4/1), pale olive (5Y 6/3), and very dark green (10YR 3/1) to greenish (unnamed—10Y 4/2). They are diffusely to sharply defined, commonly show a diffuse top but a sharp base, and appear to be of diagenetic origin. Some laminae are curved and inclined and resemble Liesegang rings. Dark green laminae bearing traces of glauconite occur in Core 119-745A-1H. One such lamina in Section 119-745A-1H-1 contains 60% clay, 25% diatoms, and 10% quartz and feldspar. Another clay-rich layer at 148 cm in Section 119-745B-4H-2 contains 50% clay, 30% diatoms, 10% radiolarians, and 10% opaque minerals.

Minor angular to subangular silt-sized grains of quartz and feldspar are disseminated throughout the subunit, and at 31.2

mbsf (Section 119-745B-4H-5, 122 cm) is an 8-mm-diameter pebble of amphibolite.

### Subunit IB

Section 119-745B-5H-3, 50 cm, through Core 119-745B-24H; depth, 37–215 mbsf.

Age: late Miocene to Quaternary.

Subunit IB is characterized by alternations of variably clay-rich diatomaceous sediments on a scale of decimeters to meters, corresponding to the smoother and rougher textures of the split surface, (similar to those in Fig. 7, but more sharply defined). The pairing of these layers is summarized in Table 3. The contrast near the top of the subunit is between diatom ooze and diatom ooze with minor clay and silt, whereas toward the bottom alternations are between clayey diatom ooze and diatomaceous clay, even though the textural contrasts remain the same. The contrast between these layers is generally sharp, although toward the base of the subunit (Core 119-745B-21H, or from about 180 mbsf downward) the boundaries are more diffuse.

Color variations are independent of these lithologies and are dominated by grays and greenish grays: very dark gray (5Y 3/1), dark gray (5Y 4/1), gray (5Y 5/1, 5Y 6/1, N5/, and 10YR 5/1), light gray (5Y 7/1), greenish gray (5GY 5/1 and 5GY 6/1), dark green (5G 4/1 and 10YR 4/2), olive gray (5Y 6/2), and pale red (2.5YR 6/2). Some diffuse horizons have a slight reddish tinge: light brownish gray (10YR 6/2), brown (10YR 5/3), reddish brown (10R 5/1), and weak red (2.5YR 5/2).

The overall composition of the sediments is characterized by extreme variability, commonly over intervals of only a few centimeters. The major constituents are 15%–80% diatoms, 5%–65% clay, 0%–7% radiolarians, and 1%–30% quartz and feldspar silt. The variation of clay content shows a good inverse correlation with diatom content (Fig. 5). The silt component follows approximately the clay trend for the upper 70 m, but not obviously so thereafter. Peaks of the terrigenous component occur at depths of about 0–70 and 145–195 mbsf. The minor components in the sediment include traces to small percentages of volcanic glass, palagonite, amphibole, glauconite, and accessory and opaque minerals. Grain sizes are variable across the sand-clay range. Most samples examined on smear slides have peaks of between 40% and 70% in the silt-size range.

The sediment is stiff and sticky and varies from homogeneous to stratified within each lithology. Weak bioturbation is evident in places, and a few burrows are in evidence, including one filled with pyrite at 67.3 mbsf (Section 119-745B-8H-5, 33 cm). Halo structures occur at around 141 mbsf (Section 119-745B-17H-2). Mottles of various colors and black (5Y 2.5/1) smears and micronodules occur at many levels. These are probably composed of iron manganese oxide.

Minor laminated zones occur at intervals through the subunit, irrespective of lithology. They range from olive green (5Y 5/2), dark gray (5Y 4/1), and very dark gray (10YR 3/1) to dark green (5G 4/1). The base of the lamina is usually sharp, whereas the top is diffuse. These features indicate a diagenetic origin. Rare laminae of grayish green (5G 5/2 and 5G 4/2) glauconite-bearing clay occur at 74.1 (Section 119-745B-9H-2), 100.5 (Section 119-745B-12H-1), 114.6 (Section 119-745B-13H-4), and 120.9 mbsf (Section 119-745B-14H-2).

Disseminated throughout the diatomaceous and clayey sediments are small amounts ( $<< 1\%$ ) of coarse sand and granules of quartz, as well as scattered pebbles. Of the latter, the most notable are an amphibolite at 149 mbsf (Section 119-745B-18H-1, 45 cm), a 15-mm-diameter granite at 123.5 mbsf (Section

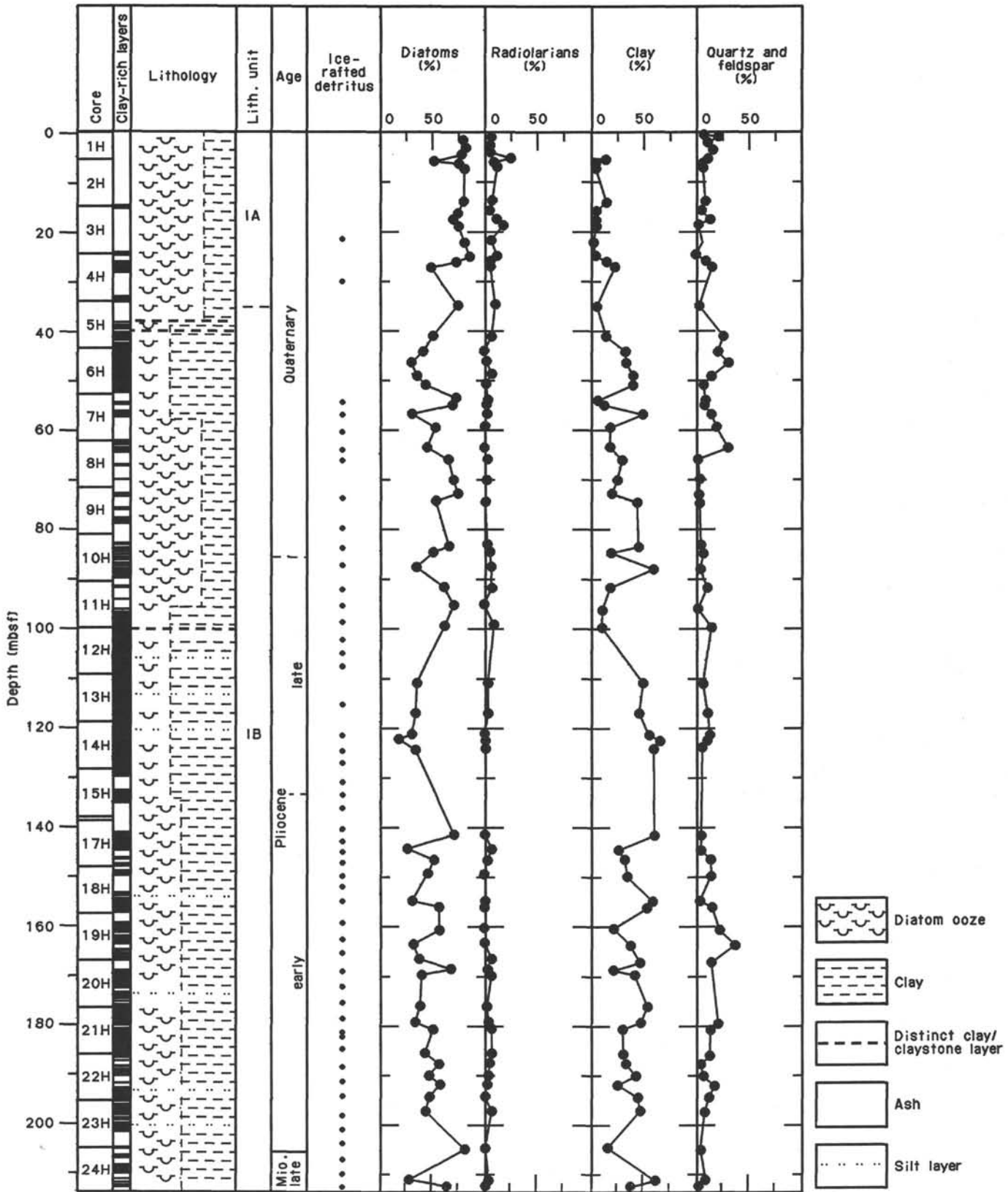


Figure 5. Summary lithostratigraphic succession at Site 745, showing ranges of clay-rich layers, and the proportions of the principal constituents of the main lithologies. Positions of lonestones (granule and larger size) of inferred ice-rafted origin are also plotted.

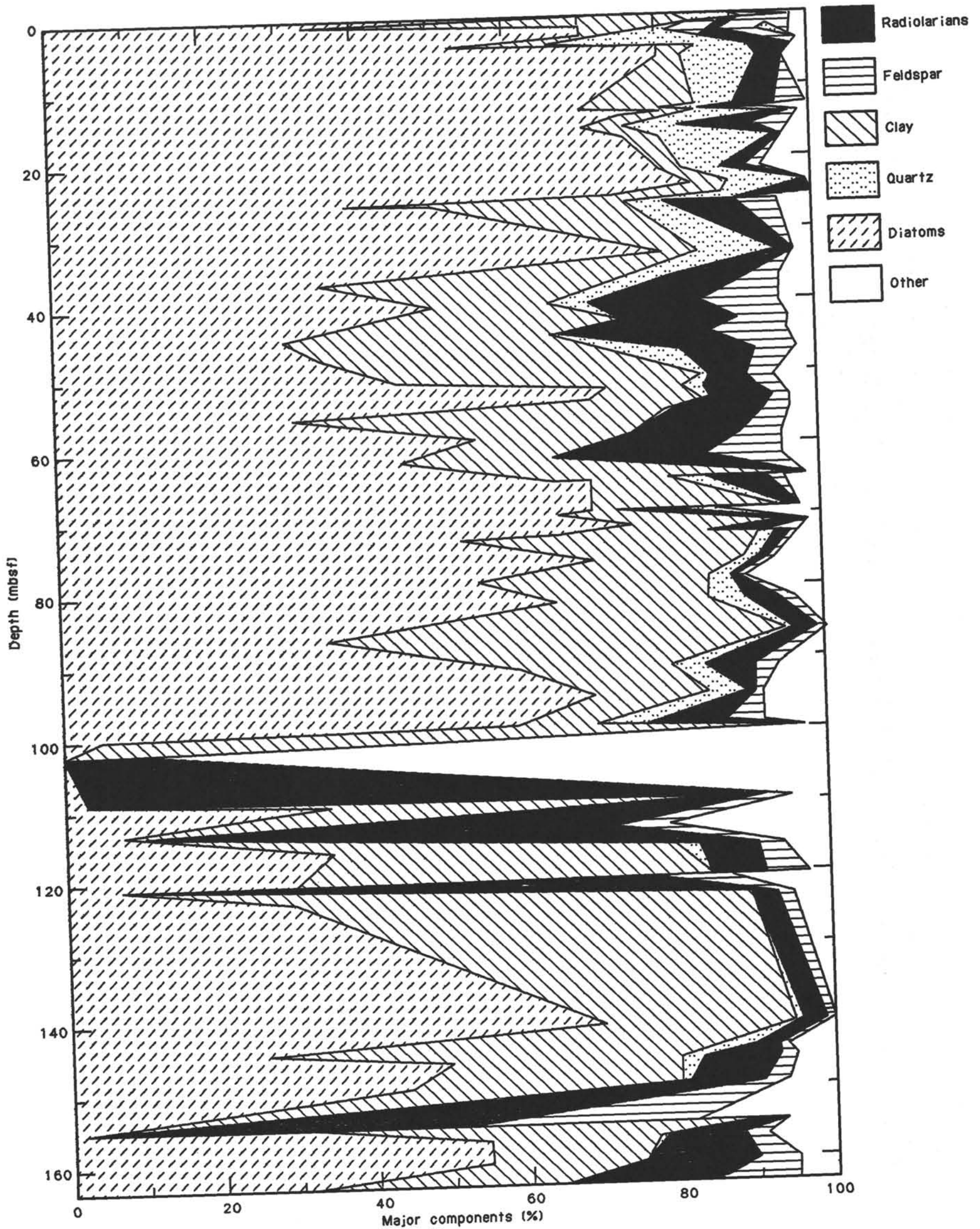


Figure 6. Cumulative percentages of major constituents from smear slide data, Site 745.

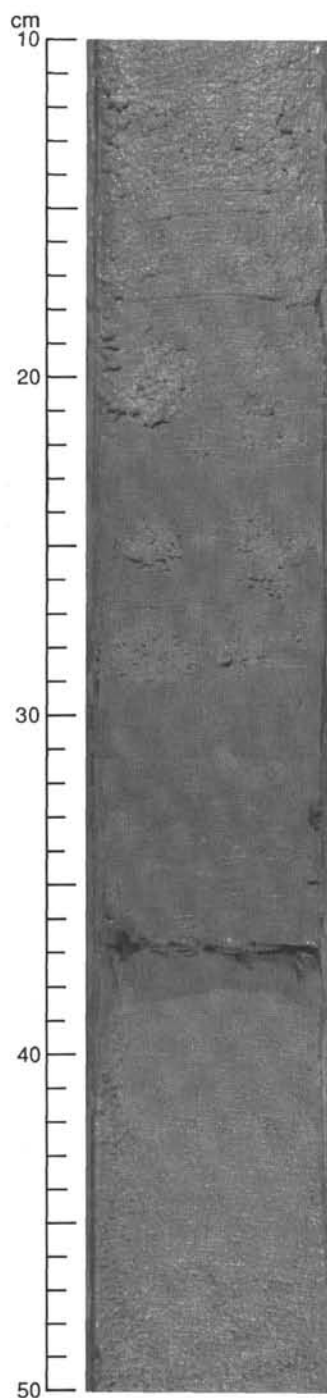


Figure 7. Alternation of clay-rich (smooth) and clay-poor (rough) layers in Subunit IA (Section 119-745B-2H-2, 10–50 cm).

119-745B-14H-4), a 5-cm-diameter gneiss at 167.6 mbsf (Section 119-745B-20H-1), and a 3-cm-diameter pellet at 173.8 mbsf (Section 119-745B-20H-5).

A number of minor lithologies are represented in the recovered sequence at various levels:

1. At 37.0, 39.2, and 39.9 mbsf (Sections 119-745B-5H-3, 130–132 cm, 119-745B-5H-4, 120 cm, and 119-745B-5H-5, 40 cm, respectively) are subcentimeter-thick layers of dark green, compacted, diatomaceous clay. One sample has the following

Table 3. Summary of pairs of clay-poor and clay-rich lithologies, represented by rough and smooth textures of the split core, Hole 745B.

Core	Clay-poor horizons	Clay-rich horizons
5H	Diatom ooze	Diatom ooze with minor clay and quartz-feldspar silt
6H and 7H	Diatom ooze	Diatomaceous silty clay to clayey diatom ooze
8H	Diatom ooze with minor quartz-feldspar silt and clay	Silty diatom ooze with minor clay
9H	Diatom ooze	Clayey diatom ooze with minor clay
10H	Clayey diatom ooze	Diatomaceous clay
11H	Diatom ooze	Diatomaceous clay
12H	Clayey diatom ooze	Diatomaceous clay
13H and 14H	Clayey diatom ooze	Diatomaceous clay with minor quartz-feldspar silt
15H	Clayey diatom ooze	Diatomaceous clay
16H	(no recovery)	
17H and 18H	Clayey diatom ooze	Diatomaceous clay
19H	Clayey diatom ooze	Diatomaceous silty clay and diatomaceous clay
20H	Clayey diatom ooze	Diatomaceous clay
21H and 22H	Clayey diatom ooze	Diatomaceous clay with minor quartz-feldspar silt
23H	Diatom ooze	Diatomaceous clay
24H	Clayey diatom ooze	Diatomaceous clay

constituents: 40% clay, 35% diatoms, 21% quartz and feldspar, and 2% opaque minerals.

2. At 100.5 mbsf (Section 119-745B-12H-1, 50–51 cm) a glauconite-bearing claystone consists of 90% clay, 5% diatoms, 1% sponge spicules, 2% quartz, 2% opaque minerals, and traces of glauconite.

3. Friable silt layers with sharp tops and bases occur at several levels: 109.3 (Section 119-745B-12H-7, 30–31 cm), 113.8 (Section 119-745B-13H-3, 133–134 cm), 121.0 (Section 119-745B-14H-2, 55–57 cm), 154.8 (Section 119-745B-18H-5, 31–32 cm), 173.0 (Section 119-745B-20H-4, 102–103 cm), and 194.1 mbsf (Section 119-745B-22H-6, 9–10 cm). These silts are well sorted (typically 0%–10% sand, 85%–90% silt, and 5%–10% clay), and they range in color from dark gray (2.5Y 4/0 and N4/) to white to reddish brown (7.5YR 5/3). Compositionally, the following proportions have been estimated from smear slides: 70%–82% quartz and feldspar, trace–12% diatoms, 0%–1% radiolarians, 0%–5% clay, 2%–10% amphibole, 0%–5% palagonite, 0%–5% glass, 1%–3% opaque minerals, and trace–3% glauconite.

4. Gray (5Y 5/1) ash layers occur at 102.5 (Section 119-745B-12H-2, 102 cm) and 173.7 mbsf (Section 119-745B-20H-5, 16–18 cm). The sand/silt/clay ratios are 50/50/0 and 10/70/20, respectively. They consist of mainly glass with some quartz-feldspar silt.

### Interpretation

Deposition at Site 745 was essentially of a mixed siliceous pelagic-terrestrial character, with practically no carbonate accumulation. Throughout most of the time interval represented by the core, sedimentation was essentially dominated by diatom ooze and clay, with a significant quartz-feldspar silt component.

Sedimentary structures are poorly developed, and most of the stratification (diffuse bedding and lamination) appears to be of diagenetic origin. The concentrations of clay may also be partly diagenetic. Although bioturbation is evident in parts of the core, it is generally diffuse, and little information concerning the species responsible can be determined. However, some distinct burrows appear in the upper cores. These sediments may be insufficiently consolidated to show such structures clearly.

The site shows marked variations in the proportions of the major components. The principal characteristic of the sequence is the alternation of more and less clay-rich zones on a scale of decimeters to meters. These have been plotted against depth (Fig. 5) to determine whether any distinct cyclicity related to glacial-interglacial cycles could have occurred. Such a determination has been made for similar sediments in the Norwegian Sea (Eldholm, Thiede, et al., 1987). However, no distinct cyclicity is apparent at Site 745. The shape of the abundance curves for diatoms and clay shows a clear inverse correlation, indicating either a steady rate of pelagic sedimentation, but variable clay sedimentation, or a suppressed rate of pelagic sedimentation as the clay component increased. The origin of the clay fraction is uncertain as yet, but some of it probably is part of an ice-rafted component, at least in the top 70 m or so, where the more obviously ice-rafted, quartz-silt component follows a roughly similar trend. Below this depth, however, no obvious relationship occurs between clay and silt, and a possible nepheloid-transport origin from the Antarctic continental margin cannot be excluded.

The evidence for the ice-rafted origin of the quartz-feldspar silt fraction is indicated by the freshness of the grains and their angular to subangular shapes. More obviously, the ice-rafted components are small pebbles of quartz-feldspar biotite gneiss, amphibolite, and granite, some of which resemble those seen in the diamictites at the Prydz Bay sites. A few show faceting, but the coarse texture of the clasts does not show striations. Such clasts could not come from a continental basement as none is nearer than the Antarctic margin. Relatively fresh-looking, heavy mineral grains that could be derived from the same suite of metamorphic rocks also indicate transport from a considerable distance by ice. The abundance of supposed ice-rafted material as a whole, however, bears no relationship to the pattern of alternating clay-rich and clay-poor layers, and we see no indication that the latter represent glacial-interglacial cycles.

The proportion of ice-rafted material in the sediment gives a crude indication of the variability of iceberg production in Antarctica. Broad, complex peaks of ice-rafted material occur from 30 to 70 mbsf and 155 to 185 mbsf, indicating enhanced glaciation in early Pliocene and Quaternary times. Nevertheless, at least some ice rafting apparently continued in late Miocene and late Pliocene times as well.

Although the sediments show little evidence of bottom current or turbidite activity, as might be expected in such a bathymetric setting, the six thin, well-sorted silt horizons may represent pulses of enhanced current activity, either through winnowing out of the normal mixed sediment during a period of nondeposition or by input during discrete events. They represent concentrations of reworked and resedimented ice-rafted material, mixed with locally derived, fragmented diatom and spicule material.

Ash layers at two levels indicate volcanic activity in the Kerguelen Plateau region sometime in early Pliocene and middle Quaternary times.

### BIOSTRATIGRAPHY

A 215.0-m-thick sequence ranging from the uppermost Miocene through the upper Quaternary was recovered at Site 745. Hole 745A was abandoned after the first core failed to preserve the mud line, and Hole 745B was abandoned because of an approaching iceberg. The sediments are composed mainly of clayey siliceous ooze deposited at 4082.5-m water depth. Foraminifers and calcareous nannofossils occur in few samples and are strongly etched because of deposition near the carbonate compensation depth (CCD). High-diversity and well-preserved diatom and radiolarian assemblages occur in all core-catcher samples in moderate to high abundance. These enable placement of the Plio-

cene/Pleistocene boundary at about 85 mbsf, the lower/upper Pliocene boundary at about 135 mbsf, and the Miocene/Pliocene boundary at about 206 mbsf (Fig. 8).

### Calcareous Nannofossils

Most core-catcher samples recovered at Site 745 were barren of nannofossils. Rare and strongly etched nannofossils, belonging to low-diversity assemblages of Neogene age, were observed in Samples 119-745A-1H-CC, 119-745B-1H-CC, 119-745B-3H-CC, 119-745B-6H-CC, and 119-745B-11H-CC.

### Foraminifers

Foraminifers from Holes 745A and 745B are present in the mud-line sample and in Sample 119-745B-4H-CC. All other core-catcher samples examined are barren of foraminifers. The surface assemblage contains a moderately abundant benthic fauna with a few planktonic specimens of *Neogloboquadrina pachyderma*. The benthic component is relatively diverse and is clearly dominated by arenaceous species. Calcareous taxa are only represented by *Pullenia bulloides*. Common agglutinated taxa include *Recurvoides scitulus*, *Hemisphaerammina bradyi*, *Reophax* spp., *Clavulina* sp., and *Bathysiphon* sp. Species such as *Cyclammina cancellata*, *Psammosphaera fusca*, *Trochammina* sp., *Cribratomoides subglobosus*, and *Rhabdammina* sp. are present in rare abundance.

Rare specimens of *Neogloboquadrina pachyderma*, *Nuttalides umbonifera*, and *Cibicidoides* sp. were found in Sample 119-745B-4H-CC. The specimens are severely etched. The scarcity of calcareous foraminifers at this site indicates a position below the foraminifer lysocline, near the CCD.

### Diatoms

Diatoms are abundant to common and well preserved to moderately well preserved in all of the core-catcher samples from Holes 745A and 745B. Standard Southern Ocean diatom biostratigraphy can be applied to these samples, indicating that the uppermost Miocene through Quaternary is represented.

Samples 119-745A-1H-CC and 119-745B-1H-CC to 119-745B-3H-CC were correlated with the upper Quaternary *Thalassiosira lentiginosa* Zone. The rare occurrence of *Actinocyclus ingens* in the latter sample was attributed to reworking. The interval from Samples 119-745B-4H-CC through 119-745B-8H-CC was assigned to the *Coscinodiscus elliptopora/Actinocyclus ingens* Zone, and it contains sparse reworked Miocene and Pliocene diatoms.

The presence of *Rhizosolenia barboi* above the last occurrence of *Coscinodiscus kolbei* in Samples 119-745B-9H-CC and 119-745B-10H-CC indicates they should be placed in the uppermost Pliocene to lowermost Pleistocene *Rhizosolenia barboi/Nitzschia kerguelensis* Zone.

Compared with the Pleistocene, the upper Pliocene at Site 745 appears to be compressed. Sample 119-745B-11H-CC is assigned to the *Coscinodiscus kolbei/Rhizosolenia barboi* Zone (1.89–2.2 Ma); Sample 119-745B-12H-CC is placed in the *Coscinodiscus vulnificus* Zone (2.2–2.49 Ma); and Sample 119-745B-13H-CC correlates with the *Nitzschia interfrigidaria* Zone (3.88–3.1 Ma). This interval contains sparse but consistent *Denticulopsis hustedtii*, which is reworked from the Miocene.

Sample 119-745B-14H-CC was assigned to the *Nitzschia praeinterfrigidaria* Zone, while Samples 119-745B-15H-CC and 119-745B-16H-CC were placed in the underlying *Nitzschia angulata* Zone. The lowermost Pliocene is represented by Samples 119-745B-17H-CC through 119-745B-21H-CC and was correlated with the uppermost part of the *Nitzschia reinholdii* Zone above the first occurrence of *Thalassiosira gracilis*.

Within this lowermost Pliocene section, reworked Miocene specimens of *D. hustedtii* increase in abundance (from rare to few). Previous Southern Ocean diatom biostratigraphic inter-

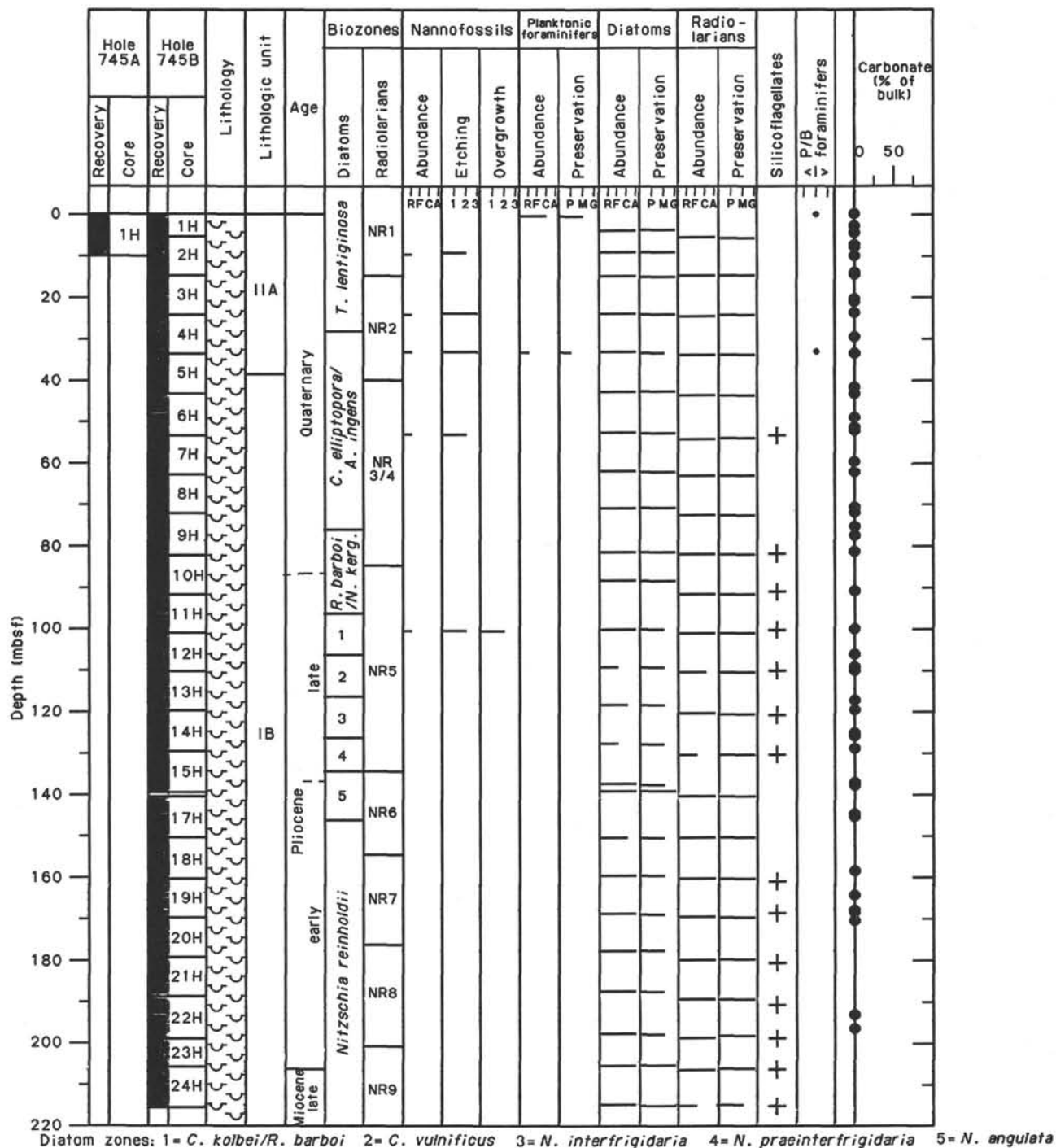


Figure 8. Biostratigraphic summary for Site 745.

pretations have indicated an early Pliocene date for the last common *D. hustedtii*. However, magnetostratigraphy at northern Kerguelen Site 737 reveals that the last common *D. hustedtii* occurred during the middle late Miocene (7.1 Ma). In addition, diatom biostratigraphy at southern Kerguelen Plateau Sites 738 and 744 shows an erosional surface at the top of the *D. hustedtii* Zone, which could act as a source for the contribution of reworked specimens of *D. hustedtii* to the deeper water Site 745.

The Miocene/Pliocene boundary (5.1 Ma) is marked by the last occurrence of *Thalassiosira miocenica* in Sample 119-745B-24H-CC. Thus, the uppermost Miocene at Site 745 is character-

ized by the presence of low-latitude *Thalassiosira* specimens, as found at Sites 737 and 738.

### Radiolarians

Radiolarians were studied in all core-catcher samples from Hole 745B. Additional samples were processed to define precise zonal limits. Very well-preserved, abundant, and highly diverse assemblages were found in all levels.

Samples 119-745B-1H-CC and 119-745B-2H-CC are correlated with the upper Quaternary NR1 Zone. They contain a typical Antarctic radiolarian assemblage. Common species include

*Antarctissa denticulata*, *Antarctissa strelkovi*, *Theocalyptra davisiana*, *Saccospyris antarctica*, and *Botryopera triloba*. Sample 119-745B-3H-3, 53–55 cm, contains many specimens of *Stylactrus universus* and falls within the NR2 Zone. The last common occurrences of *Anthocyrta callopisma* and *Phormostichoartus pitomorphus* in Sample 119-745B-5H-CC are diagnostic of the NR3/4 Zone. Samples 119-745B-5H-CC through 119-745B-9H-CC also fall within the NR3/4 Zone. The radiolarian assemblage observed in these samples is repetitious, but many last occurrences can be recognized, including the last common occurrence of *Saturnalis circularis* in Sample 119-745B-5H-6, 53–55 cm. Reworked specimens, including the Pliocene species *Stichocorys peregrina* and *Clathrocyclas bicornis*, are more abundant in Sample 119-745B-6H-CC. *Anthocyrta callopisma* appears to be consistently present in all lower Quaternary assemblages.

Samples 119-745B-10H-1, 53–55 cm, through 119-745B-14H-CC are dated as late Pliocene, falling within the NR5 Zone. Typical upper Pliocene Antarctic radiolarians, dominated by *Antarctissa ewingi* and *C. bicornis*, are present. The first appearance of *Theocalyptra davisiana* and the last common occurrence of *Desmospyris spongiosa* occur in Sample 119-745B-13H-2, 53–55 cm. Samples 119-745B-15H-3, 53–55 cm, and 119-745B-18H-4, 53–55 cm, were assigned to the lower Pliocene NR6 Zone based on occurrence of the species *Pseudocubus vema*, *D. spongiosa*, and *Prunopyle titan*. Rare specimens of *Lamprocyrtis heteroporos* are present in Sample 119-745B-15H-CC. Radiolarian assemblages in Samples 119-745B-18H-CC and 119-745B-19H-CC contain many specimens of *Helotholus(?) praeveva* and are related to the NR7 Zone. The first common occurrence of *D. spongiosa* is between Samples 119-745B-20H-5, 53–55 cm, and 119-745B-20H-6, 53–55 cm. Thus, the interval between core-catcher Samples 119-745B-20H-CC and 119-745B-22H-CC falls within the NR8 Zone. Samples 119-745B-23H-CC and 119-745B-24H-CC are tentatively dated as early Pliocene because of the occurrence of many specimens of *S. peregrina* along with many representatives of *H.(?) praeveva* and *Lychnocanium*.

### Palynomorphs

No samples were processed for palynomorphs at this site.

### PALEOMAGNETICS

Hole 745B was cored using the APC, and the sedimentary sequence samples consist of diatom ooze. The natural remanent magnetization (NRM) was measured on the archive halves of Cores 119-745B-1H to 119-745B-24H and on 327 discrete samples using the shipboard cryogenic magnetometer.

Figure 9 shows plots of NRM directions and intensities for the samples from Hole 745B. The NRM intensities vary between 0.6 and 161 mA/m. Many short-range fluctuations in NRM intensities are present within this sedimentary sequence. NRM intensities show a decreasing trend from 110 mbsf downward in the hole.

Magnetic measurements show good correlation with the magnetic reversal scale of Berggren et al. (1985). NRM inclinations are plotted against depth downhole in Figure 10. The inclination data show the location of the Chron C1N/C1R (Brunhes/Matuyama Chronozones) boundary in Section 119-745B-6H-6 (43 mbsf). The sediments below this boundary down to 124 mbsf are characterized by reverse polarity and are assigned to the Matuyama reverse polarity zone. Two normal polarity subzones, between 51 and 54 mbsf and between 90 and 93 mbsf, are correlated to Subchrons C1R-1 (Jaramillo Subchronozones) and C2 (Olduvai Subchronozones), respectively. Normal inclinations at 56 mbsf may be the split Jaramillo Event. Further information should be available after a shorebased demagnetization examination.

A normal polarity zone between 113 and 130 mbsf is assigned to C2A (Gauss Chronozones). The reversal zones in this zone may be correlated to the Mammoth and Kaena Subchrons.

Below 135 mbsf, the correlation of the magnetic polarity zones with standard geomagnetic reversal sequences is not clear. Detailed shorebased demagnetization studies will be necessary to define the sequence.

### SEDIMENTATION RATES

The clayey siliceous ooze recovered from Site 745 was deposited at an average rate of 30 m/m.y. from the surface to the base of the sequence (215 mbsf), which is considered latest Miocene in age. This rate was determined from the age estimates and depth intervals of various biostratigraphic events listed in Table 4 and the sub-bottom depths of the Site 745 polarity reversals (Fig. 11). The biostratigraphic events are plotted against depth below seafloor in Figure 11. Although the current resolution is limited to core-catcher samples, the plot indicates that either a hiatus occurs between 109.5 and 119.0 mbsf (2.22–3.88 Ma) or the first-appearance datums for the diatom species *Nitzschia weaveri*, *Nitzschia interfrigidaria*, and *Nitzschia angulata* are too old.

### INORGANIC GEOCHEMISTRY

Two holes were cored in 4082.5 m of water at Site 745 on the southeastern slope of the southern Kerguelen Plateau. Ten whole-round minicores 5 cm in length were obtained from 3 to 192 mbsf for the purpose of interstitial-water chemical studies. The sediment minicores consist of lower Pliocene to Quaternary silty diatom ooze and diatom clay (see "Lithostratigraphy and Sedimentology" section, this chapter) and contain 0%–0.2% calcium carbonate and 0.1%–0.4% organic carbon (see "Organic Geochemistry" section).

### Results

Site 745 interstitial-water samples were analyzed for pH, alkalinity, salinity, chloride, sulfate, magnesium, calcium, phosphate, ammonium, and silica using the methods outlined in the "Explanatory Notes" chapter. Charge-balance calculations were performed on each of the interstitial-water samples to check for gross irregularities in the data. Sodium and potassium were calculated by multiplying the ratio of each cation to chloride for average seawater, using the values given by Stumm and Morgan (1981), by the chloride concentration of each sample. All of the samples have charge imbalances less than 2%, confirming that drilling contamination was minimal. All of the data obtained at Site 745 are shown in Table 5.

#### Salinity and Chloride

The salinity and chloride concentration of the interstitial waters at Site 745 do not change appreciably from 3 to 192 mbsf (Fig. 12). A small downhole increase in salinity and chloride concentration is indicated between 3 and 20 mbsf, but the increase is within the range of analytical precision. The mean salinity (35.7 g/kg, s.d. = 0.3 g/kg, n = 10) and mean chloride concentration (555 mmol/L, s.d. = 3 mmol/L, n = 10) of this set of samples are probably similar to the composition of ocean bottom water at this site.

#### Magnesium and Calcium

Interstitial-water magnesium and calcium concentrations are well correlated ( $r = -0.990$ ) between 3 and 192 mbsf at Site 745 (Fig. 12). Dissolved magnesium concentrations decrease 30%, and dissolved calcium concentrations increase 81% with increasing depth from 3 to 192 mbsf. The linear correlation between magnesium and calcium implies that these cations behave conservatively in the portion of the sediment column sampled

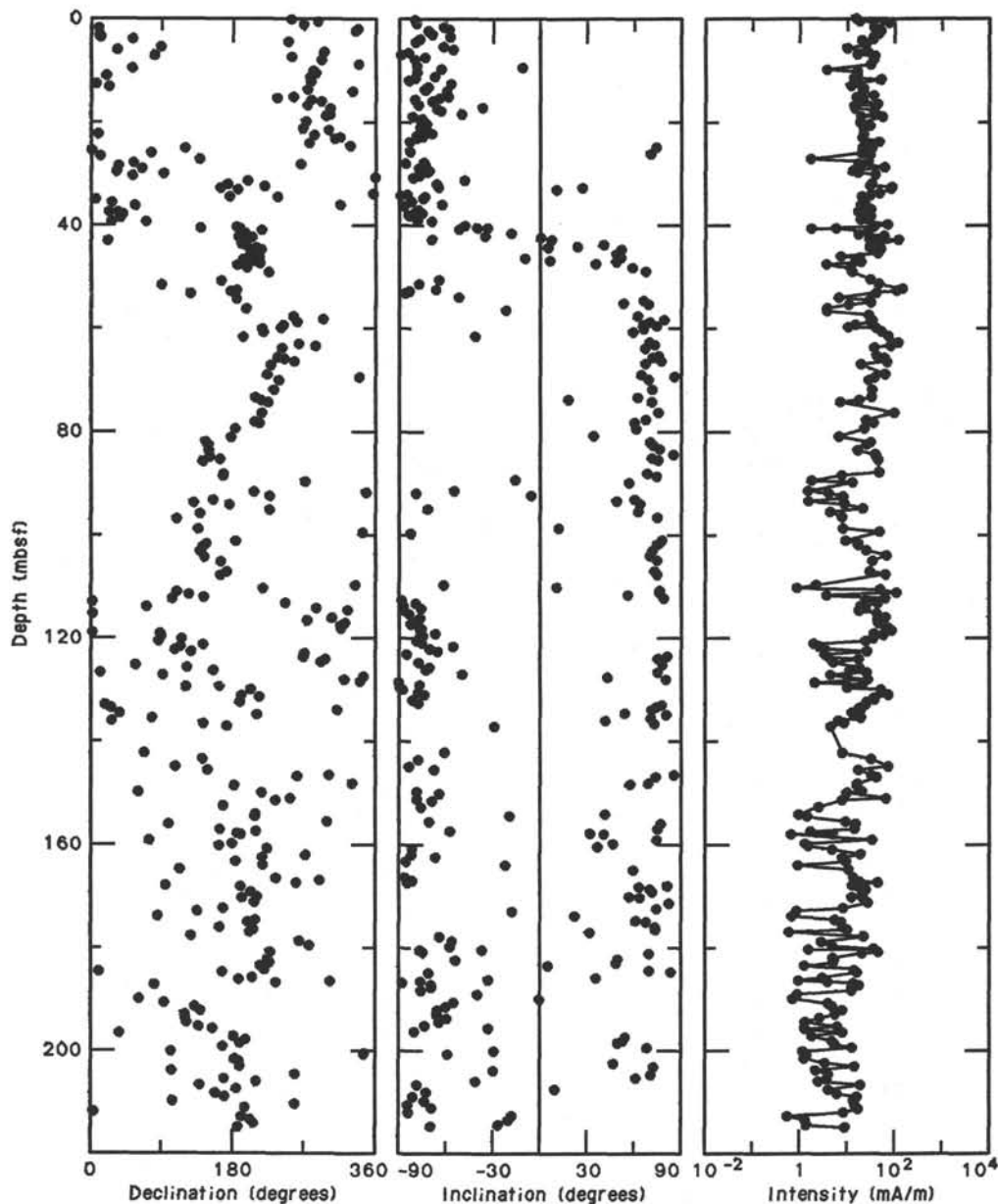


Figure 9. Profiles of magnetic declination, inclination, and intensity, Hole 745B.

for this study (see McDuff and Gieskes, 1976; McDuff, 1978; Gieskes, 1983). Dissolved magnesium enters the sediment column at the seafloor and is generally consumed during the alteration of basement rocks. Calcium is produced during reactions between pore fluids and rocks below 192 mbsf and diffuses through the sediments to the ocean reservoir. The relatively small slope ( $-0.48$ ) of the regression line passing through the data points representing the calcium and magnesium concentrations of the interstitial-water samples (Fig. 13) indicates that magnesium is being consumed more rapidly than calcium is being produced by water-rock reactions below 192 mbsf.

#### Silica

The concentration of silica in the interstitial waters at Site 745 steadily increases with increasing depth from 3 to 192 mbsf (Fig. 12). Dissolution of biogenic silica in the sediments results in a 37% increase in dissolved silica concentrations between 3

and 192 mbsf. The concentration of dissolved silica at 3 mbsf is approximately 10 times greater than in surface seawater in this area. Thus, the dissolution of biogenic silica in the sediments at Site 745 supplies silica to the ocean reservoir as part of the continual cycling of silica in the ocean.

#### pH, Alkalinity, Sulfate

The pH, alkalinity, and sulfate analyses of interstitial-water samples indicate that small amounts of reactable organic matter are being incorporated into the sediments at Site 745 (Fig. 12). The variation in pH values between 3 and 192 mbsf is the same as the analytical precision, indicating that the interstitial waters are being buffered at their mean value of 7.5 (s.d. = 0.1,  $n = 10$ ). Alkalinity doubles with increasing depth between 3 (3.4 mmol/L) and 192 mbsf (6.8 mmol/L). This increase can be attributed to the production of base compounds such as bisulfide, bicarbonate, and phosphate during bacterial catabolism. Alka-

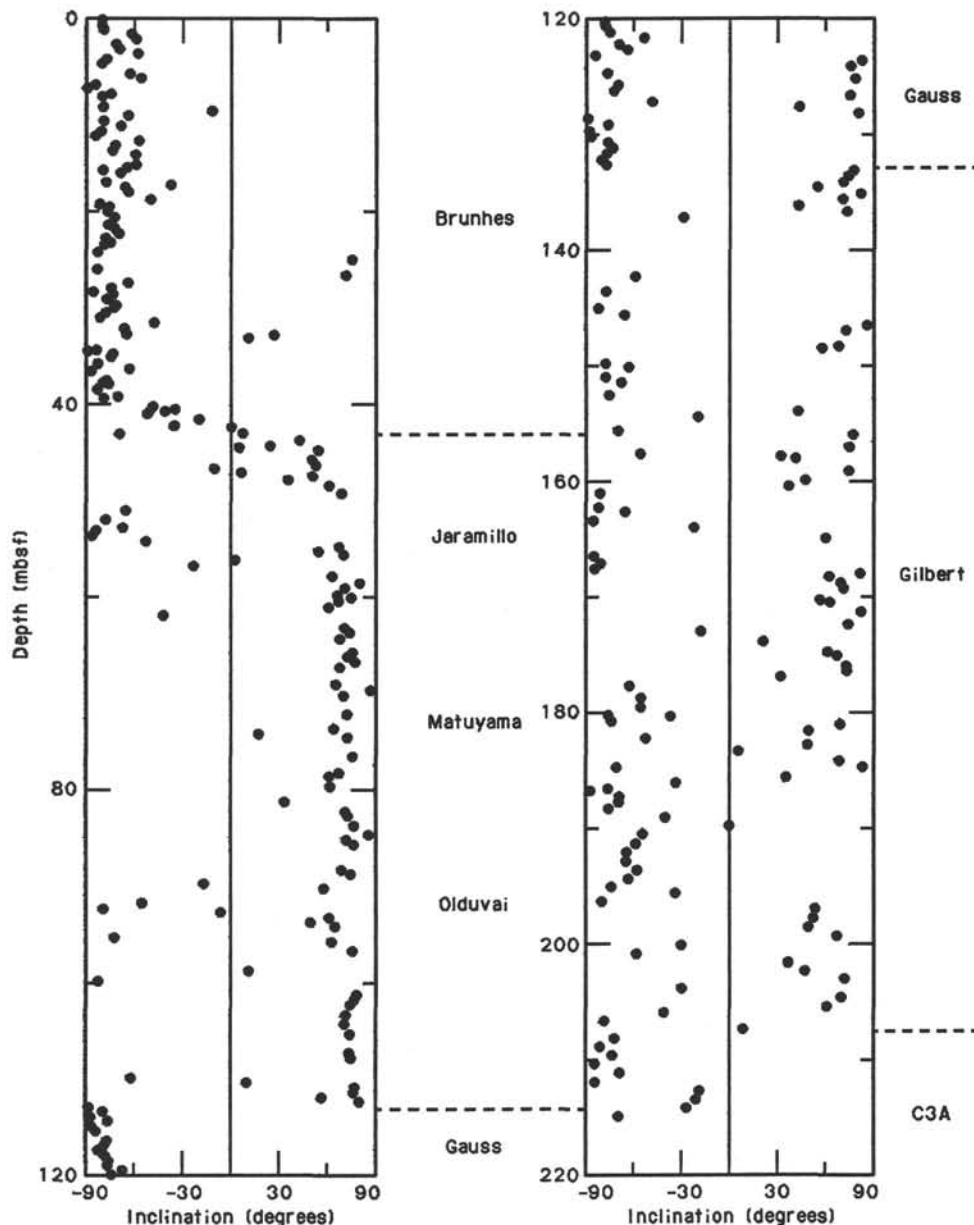


Figure 10. Magnetic inclination and assigned polarity (Berggren et al., 1985), Hole 745B.

linity values are relatively constant (mean = 6.38, s.d. = 0.26,  $n = 7$ ) from 49 to 192 mbsf, indicating that most of the microbial biodegradation is confined to the uppermost 49 mbsf at this site. Interstitial-water sulfate concentrations steadily decrease from 29.4 mmol/L at 8 mbsf to 19.4 mmol/L at 192 mbsf. This decrease implies that either bacterial sulfate reduction occurs throughout this depth interval or that the main zone of sulfate reduction occurs at a deeper level in the sediment column. The gradual decline in sulfate concentration with depth supports the latter possibility. The fact that the concentration of sulfate is still decreasing at 192 mbsf requires that sulfate reduction continue below this depth.

#### Ammonium and Phosphate

Ammonium and phosphate concentrations in the interstitial waters at Site 745 indicate that the most intense zone of bacterial activity occurs between 3 and 49 mbsf (Fig. 12). Dissolved ammonium concentrations increase with increasing depth from

3 to 192 mbsf, with the majority of the increase occurring in the uppermost 49 mbsf. Phosphate concentrations peak at 20 mbsf ( $23 \mu\text{mol/L}$ ) and then decrease with depth before leveling off at 106 mbsf ( $4 \mu\text{mol/L}$ ). The phosphate maximum indicates that microbial catabolism is most intense at 20 mbsf. The concentration vs. depth profiles of dissolved phosphate and sedimentary organic carbon (see "Organic Geochemistry" section) are remarkably similar, implying that microbial activity at shallow depths plays an important role in determining the final organic carbon content of deeply buried sediments. Increasing ammonium concentrations from 125 to 192 mbsf support the belief that bacterial sulfate reduction occurs below 192 mbsf.

#### ORGANIC GEOCHEMISTRY

Hole 745B was drilled to 215.0 mbsf in 4082.5 m of water. Hole 745A was only one core, 0.5–10.5 mbsf, as the mud line was missed. Organic geochemical analyses were done on squeeze cakes from interstitial-water samples, core-catcher samples, and

Table 4. Bioevents identified at Site 745.

Biostratigraphic event <sup>a</sup>	Depth (mbsf)	Age (Ma)
LAD <i>Stylatractus universon</i>	16.5–31.8	0.42
LAD <i>Actinocyclus ingens</i>	24.0–33.5	0.65
LAD <i>Rhizosolenia barboi</i>	71.5–81.0	1.58
LAD <i>Clathrocyclas bicornis</i>	84.5–86.0	1.6–1.8
LAD <i>Coscinodiscus kolbei</i>	90.5–100.0	1.89
LAD <i>Coscinodiscus vulnificus</i>	100.0–109.5	2.22
FAD <i>Theocalyptra davisiana</i>	111.5–113.0	2.5–2.6
LAD <i>Prunipyle titan</i>	130.0–132.0	3.2
FAD <i>Nitzschia weaveri</i>	119.0–128.5	3.2–3.3
FAD <i>Nitzschia interfigidaria</i>	128.5–137.5	4.02
FAD <i>Nitzschia angulata</i>	139.0–148.5	4.2
FAD <i>Pseudocubus vema</i>	153.0–155.0	3.95
LAD <i>Tricerapys coronata</i>	164.0–165.0	4.25
FAD <i>Desmospyris spongiosa</i>	174.0–175.0	4.3
LAD <i>Stichocorys peregrina</i>	201.0–202.0	4.4–4.6
FAD <i>Thalassiosira gracilis</i>	186.5–196.0	4.6–4.7
LAD <i>Thalassiosira miocentica</i>	205.5–215.0	5.1

<sup>a</sup> FAD = first-appearance datum; LAD = last-appearance datum.

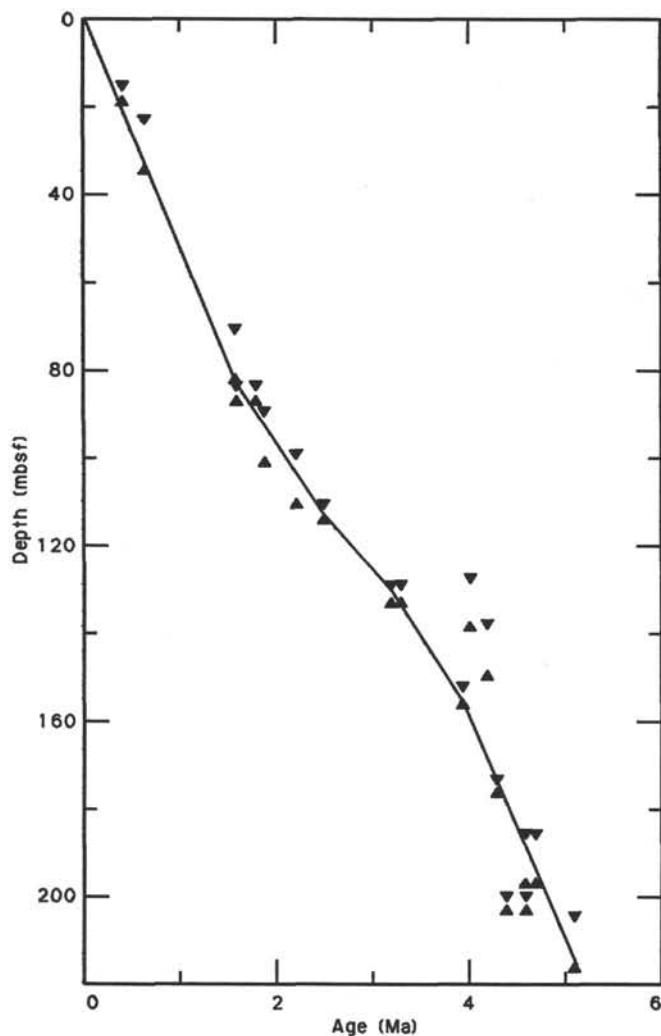


Figure 11. Age vs. depth profile based on biostratigraphic events, Site 745.

physical-properties samples. The methods and instruments used are described in the "Explanatory Notes" chapter.

### Hydrocarbon Gases

The headspace procedure was used approximately every 30 m. Methane was the only hydrocarbon detected, and it was only found at very low levels (23 ppm or less) at Site 745.

### Carbon Analysis

Carbonate analysis was performed on all of the samples using the coulometric method detailed in the "Explanatory Notes" chapter. Total carbon analysis was done on the squeeze-cake samples from the interstitial-water studies. Table 6 is a summary of the carbon data. Figure 14 is a plot of carbonate and organic carbon percentages.

There are only trace amounts of carbonate at Site 745. Organic carbon is 0.3%–0.4% in the top of the hole, and decreases to about 0.1% at 100 mbsf, where it remains near 0.1% downhole.

### Rock-Eval Pyrolysis

Rock-Eval pyrolysis was performed on the squeeze cakes from interstitial-water studies that were used for total carbon analysis. The parameters measured and calculated are listed in Table 7 and shown graphically in Figures 15 through 18. Figure 18 is a modified van Krevelen plot of the oxygen index vs. hydrogen index.

As at the other Kerguelen sites analyzed, the  $T_{max}$  value ranged from immature to very mature. One explanation could be intensive reworking of the marine material along with terrestrial input (Tissot and Welte, 1984). Doublet S2 peaks indicate likely input from more than one source, possibly because of reworking of the organic matter.

The kerogen is a mixture of type II and type III. Figure 18 shows that all the samples appear to have both marine and terrestrial carbon except Sample 119-745A-12H-4, 145–150 cm, which may contain only marine carbon.

Sample 119-745A-1H-2, 145–150 cm, appears to have only terrestrial carbon and is only slightly mature. This is unlikely, as it is in a marine environment. This sample probably reflects deposition in oxic conditions. Samples of marine origin deposited in oxic conditions were found by Deroo et al. (1978, 1979) on Deep Sea Drilling Project Legs 44 in the Blake-Bahama Basin and 48 in the Bay of Biscay.

## BIOLOGY AND OCEANOGRAPHY

### Physical Characteristics of the Air/Sea Interface

Brisk winds shifted from east-northeast, then southeast to southwest, and back to north and northeast over the study period at the two adjacent Sites 745 and 746 (8–11 February), decreasing to calm (11 February; see Table 8). From 8 to 11 February, the sea-surface temperature at the drill ship ranged from +1.5° to +2.0°C. Records transcribed from traces of expendable bathythermographs deployed from the drill ship after completion of nearby Site 746 are shown (Fig. 19), because bathythermographs used in transit to Site 745 left faulty traces.

### Phytoplankton

The phytoplankton was sampled daily off the stern of the *JOIDES Resolution* by use of a hand-held 20- $\mu$ m-mesh net fished for 5 min in the effluent from the thrusters. Diverse species found over the study period are shown in Table 9. Although the same flora was present, the amount of the collection and the dominant species changed from day to day.

Throughout the study period, *Asteromphalus* species, especially the smallest species, *Asteromphalus hyalinus*, were abundant. Although this is a common species in Antarctic material,

Table 5. Interstitial-water geochemical data, Site 745.

Core, section, interval (cm)	Depth (mbsf)	Volume (mL)	pH	Alkalinity (mmol/L)	Salinity (g/kg)	Magnesium (mmol/L)	Calcium (mmol/L)	Chloride (mmol/L)	Sulfate (mmol/L)	Phosphate ( $\mu\text{mol/L}$ )	Ammonium (mmol/L)	Silica ( $\mu\text{mol/L}$ )	$\text{Mg}^{2+}/\text{Ca}^{2+}$
119-745A-													
1H-5, 145-150	7.95	47	7.5	4.00	35.5	52.7	11.2	553	29.4	20	0.10	689	4.7
119-745B-													
1H-2, 145-150	2.95	47	7.5	3.39	35.5	52.3	10.4	549	29.4	13	0.03	735	5.0
3H-4, 145-150	20.45	55	7.6	5.07	36.2	51.9	11.9	555	28.4	23	0.18	728	4.4
6H-4, 145-150	48.95	62	7.6	6.28	36.0	48.0	13.5	557	25.9	18	0.31	794	3.6
9H-4, 145-150	77.45	60	7.4	6.70	35.5	46.0	15.1	558	24.8	7	0.36	761	3.0
12H-4, 145-150	105.95	60	7.4	6.77	36.0	42.6	16.0	559	23.2	4	0.40	913	2.7
14H-4, 145-150	124.95	60	7.4	6.41	35.8	40.7	16.7	555	22.0	4	0.36	996	2.4
17H-4, 145-150	144.95	55	7.5	6.11	35.8	39.9	17.5	555	21.6	4	0.39	946	2.3
19H-4, 145-150	163.95	60	7.4	6.18	35.2	38.2	18.0	555	21.2	4	0.44	1005	2.1
22H-4, 145-150	192.45	55	7.3	6.24	35.5	36.6	18.8	556	19.4	4	0.46	1010	1.9

it was not as abundant in past collections as it was from the surface waters at Sites 746 and 739 (collection by small boat near iceberg), perhaps because of its small size. It has been effectively collected with the small-meshed net, and for the first time, sufficient numbers are available to assess its size variation and relationship with *Asteromphalus parvulus*.

The first day on Site 745 (8 February), *Rhizosolenia hebetata* f. *semispina* was abundant, and the next day the sample was somewhat reduced, with *Nitzschia cylindrus* dominant, especially in relation to deteriorating fecal pellets. Quite a change occurred on 10 February with a heavily pigmented sample. *A. hyalinus* and *A. parvulus* were still common, but large-celled *Chaetoceros* species, especially *Chaetoceros castracanei*, were in long chains. The delicate cylindrical diatom, *Dactyliosolen tenuijunctus*, both straight and coiled cells, dominated the collection, along with many specimens of *Thalassiosira lentiginosa*. The following day, the two samples taken were sparse and quite diverse, with many empty cells. Many delicate *Chaetoceros* in single cells and short chains with long, threadlike, flexible setae were present. Early on 12 February, the last sample taken was full of healthy cells, dominated by a small, single-celled *Chaetoceros* and *Dactyliosolen tenuijunctus*. Also abundant were *Chaetoceros* sp. cf. *dichaeta*, *Nitzschia cylindrus*, and *Nitzschia clostrium*.

#### Diatoms in Surface Sediments

Surface sediments had many diatom fragments and showed some evidence of reworking. Dominant species were *Nitzschia kerguelensis* and *Thalassiosira lentiginosa*. Variation in size of *N. kerguelensis* is quite marked in these sediments (Fig. 20). A shorebased study can provide similar figures from measurements made from the permanent mounts of plankton samples from different geographical areas represented by the northern and southern Kerguelen Plateau areas and Prydz Bay. In the southern Atlantic, a latitudinal gradient of size and, particularly, shape may occur. Development of an index of heteropolarity, plotted against the ratio of length/width would be helpful; an index may be possible with two additional measurements per valve. Although such microscopic measurements would be cumbersome, they could be effectively facilitated by using rapid printing of hard copies on heat-sensitive paper from a televised image. A printer was demonstrated aboard the *JOIDES Resolution* and could be an aid for shape analysis, especially if used with a digitizing tablet.

Those planktonic species noted in the surface sediment are identified in Table 9. Others seen only in the sediment include *Actinocyclus* sp. cf. *ingens*, *Azpeitia tabularis*, *Chaetoceros* resting spores (one specimen is 10  $\mu\text{m}$  long, 6  $\mu\text{m}$  wide; another is 17  $\mu\text{m}$  long), and *Thalassiosira gravida* (vegetative cells).

#### PHYSICAL PROPERTIES

The primary objectives of the physical-properties program at Site 745 were (as at Sites 736 through 738 and 744) to contribute to an understanding of syndepositional and post-depositional processes, particularly with regard to establishing the presence and nature of hiatuses and lithologic boundaries in the sediments on the Kerguelen Plateau. Also of special interest is the geotechnical response of silica-rich sediments. The shipboard-acquired data will be incorporated into a shorebased study of permeability and consolidation properties of these sediments. Physical properties measured were (1) index properties (water content, porosity, wet- and dry-bulk density, and grain density), (2) undrained shear strength, (3) compressional-wave velocity, (4) thermal conductivity, and (5) downhole temperature. Laboratory procedures and techniques are discussed in the "Explanatory Notes" chapter.

Two holes, 745A and 745B, were drilled with the APC at Site 745 to 10.5 and 215 mbsf, respectively, with excellent core recovery in Hole 745B, but some coring disturbance.

All physical-properties data for Site 745 are presented in Table 10 and Figure 21, except for the temperature data, which are presented in Table 11 and Figures 22 and 23.

#### Results

Two geotechnical units, G1 and G2, have been tentatively defined on the basis of the character and trends of physical-properties profiles and changes in lithology. These criteria also have been used to define five subunits (G1A, G1B, G2A, G2B, and G2C) within the sedimentary section. The geotechnical subunits defined are not distinguishable in terms of lithology but do have distinctive physical-property trends on one or more physical-properties depth profiles.

Geotechnical unit G1 (0-45 mbsf) is a diatomaceous ooze (see "Lithostratigraphy and Sedimentology" section). The physical-properties profiles exhibit little overall change in character or gradient, although small-scale variation is present. Bulk densities average 1.35  $\text{g}/\text{cm}^3$  with a trend of slight increase with depth. Water content and porosity decrease slightly with depth and average 65% and 80%, respectively. Compressional-wave velocity profiles change very slightly with depth and average 1500 m/s, with little scatter. Thermal conductivity is constant and averages 0.75  $\text{W}/\text{m}/^\circ\text{C}$ . Undrained shear-strength profiles show a trend of gradual increase throughout unit G1. A small-scale reversal of gradients is evident on index-properties profiles (particularly GRAPE density) at 5 mbsf, which serves to divide unit G1 into geotechnical subunits G1A and G1B.

Unit G2 (45-215 mbsf) is a diatomaceous, silty clay. The contact with overlying unit G1 is gradational but distinguish-

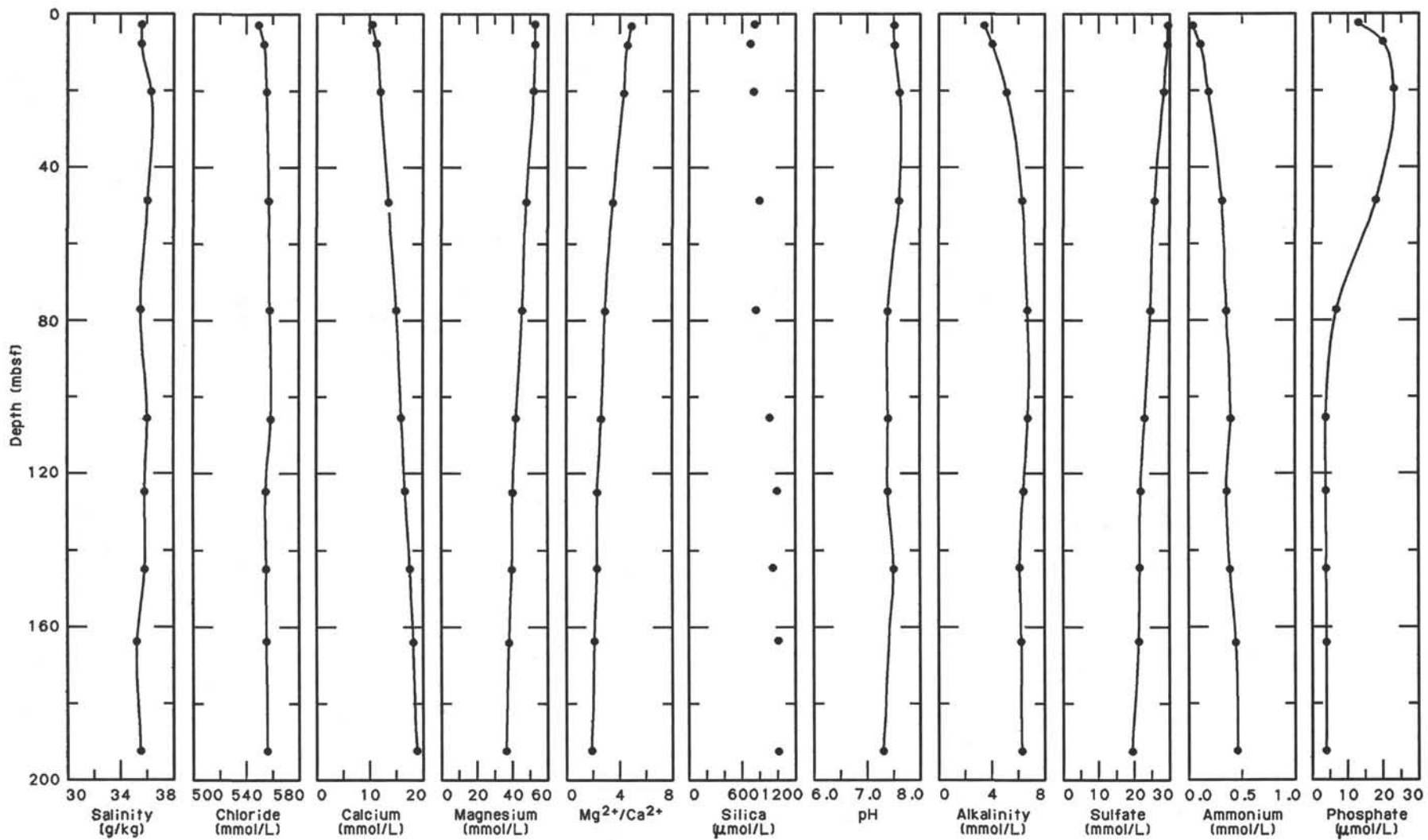


Figure 12. Interstitial-water profiles, Site 745.

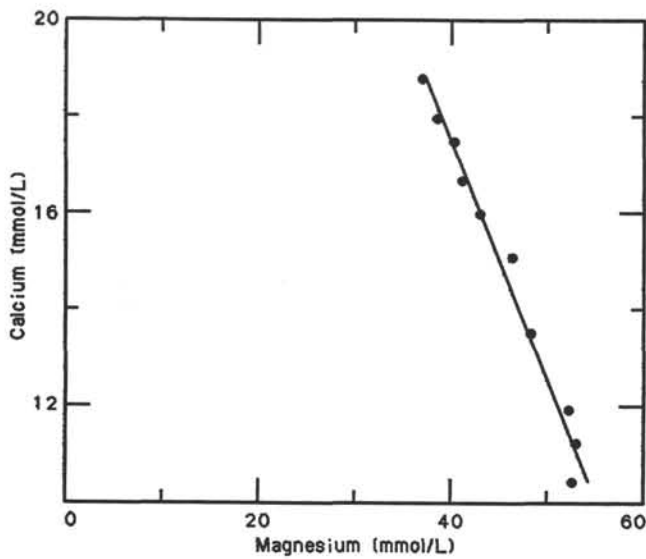


Figure 13. Calcium concentration vs. magnesium concentration for Site 745 interstitial waters. The regression line passes through data points representing interstitial-water samples in the upper 192 mbsf and has a slope of  $-0.48$  ( $r = -0.990$ ).

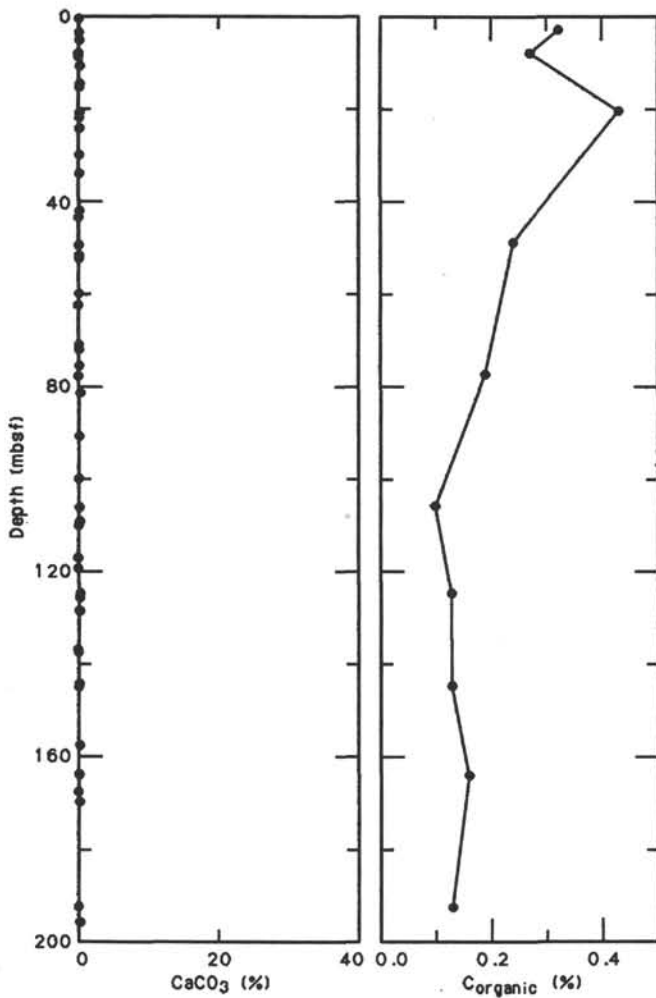


Figure 14. Carbonate and organic carbon profiles, Site 745.

Table 6. Total carbon, inorganic carbon, organic carbon, and carbonate carbon, Site 745.

Core, section, interval (cm)	Depth (mbsf)	Total carbon (%)	Inorganic carbon (%)	Organic carbon (%)	CaCO <sub>3</sub> (%)
119-745B-					
1H-1, 0-1	0.00		0.01		0.1
1H-2, 145-150	2.95	0.33	0.01	0.32	0.1
1H-3, 140-141	4.40		0.02		0.2
119-745A-					
1H-5, 90-91	7.40		0.01		0.1
1H-5, 145-150	7.95	0.28	0.01	0.27	0.1
1H-CC, 0-1	10.12		0.01		0.1
119-745B-					
2H-7, 16-18	14.16		0.01		0.1
2H-CC, 0-1	14.61		0.01		0.1
3H-4, 145-150	20.45	0.44	0.01	0.43	0.1
3H-5, 80-80	21.30		0.01		0.1
3H-CC, 0-1	23.80		0.01		0.1
4H-4, 112-113	29.62		0.01		0.1
4H-CC, 0-1	33.65		0.02		0.2
5H-6, 80-82	41.80		0.02		0.2
5H-CC, 0-1	43.20		0.01		0.1
6H-4, 145-150	48.95	0.25	0.01	0.24	0.1
6H-6, 90-92	51.40		0.02		0.2
6H-CC, 0-1	52.11		0.01		0.1
7H-5, 120-121	59.70		0.01		0.1
7H-CC, 0-1	62.14		0.01		0.1
8H-6, 115-116	70.65		0.01		0.1
8H-CC, 0-1	71.71		0.04		0.3
9H-3, 69-70	75.19		0.02		0.2
9H-4, 145-150	77.45	0.20	0.01	0.19	0.1
9H-CC, 0-1	81.21		0.02		0.2
10H-7, 40-41	90.40		0.01		0.1
10H-CC, 0-1	90.69		0.01		0.1
11H-7, 20-21	99.70		0.01		0.1
11H-CC, 0-1	99.95		0.02		0.2
12H-4, 145-150	105.95	0.12	0.02	0.10	0.2
12H-7, 13-14	109.13		0.02		0.2
12H-CC, 0-1	109.77		0.02		0.2
13H-6, 6-7	117.06		0.02		0.2
13H-CC, 0-1	119.24		0.01		0.1
14H-4, 145-150	124.95	0.14	0.01	0.13	0.1
14H-5, 70-71	125.70		0.01		0.1
14H-CC, 0-1	128.64		0.02		0.2
15H-6, 88-89	136.88		0.01		0.1
15H-CC, 0-1	137.36		0.01		0.1
17H-4, 90-92	144.40		0.01		0.1
17H-4, 145-150	144.95	0.13	0.00	0.13	0.0
18H-7, 35-37	157.85		0.02		0.2
19H-4, 145-150	163.95	0.17	0.01	0.16	0.1
19H-7, 50-51	167.50		0.01		0.1
19H-CC, 0-1	167.78		0.01		0.1
20H-2, 80-83	169.80		0.01		0.1
22H-4, 145-150	192.45	0.15	0.02	0.13	0.2
22H-7, 5-6	195.55		0.02		0.2
22H CC, 0-1	195.75		0.02		0.2

able by slight changes in gradients on physical-properties profiles. It is most clearly evident on the GRAPE density plot. Overall, data are fairly constant with depth in geotechnical unit G2 and only slightly different from unit G1 average values—55% water content, 70% porosity, and 1.45 g/cm<sup>3</sup> density. Unit G2 is subdivided into three subunits based on gradient reversals of index-property and shear-strength profiles. Velocity and thermal conductivity are essentially constant with depth, with the same average values as in unit G1.

Subunit G2A (45-80 mbsf) is distinguishable on index-property profiles as a trend of reversed gradients. Densities decrease, whereas porosity and water content increase slightly with depth. Undrained shear-strength gradients change, but do not reverse, to a trend of constant average values with depth.

Table 7. Rock-Eval summary, Site 745.

Core, section, interval (cm)	Depth (mbsf)	Weight (mg)	T <sub>max</sub> (°C)	S1 (mg HC/g)	S2 (mg HC/g)	S3 (mg CO <sub>2</sub> /g)	Productivity index	S2/S3	Pyrolyzied carbon (0.08 [S1 + S2])	TOC (wt%)	Hydrogen index (mg HC/g C <sub>org</sub> )	Oxygen index (mg CO <sub>2</sub> /g C <sub>org</sub> )
119-745B-												
1H-2, 145-150	2.95	100.1	443	0.11	0.50	0.58	0.18	0.86	0.05	0.32	156	181
119-745A-												
1H-5, 145-150	7.95	100.4	472	0.35	0.90	0.47	0.28	1.91	0.10	0.27	333	174
119-745B-												
3H-4, 145-150	20.45	97.5	370	0.48	1.11	0.57	0.30	1.94	0.13	0.43	258	132
6H-4, 145-150	48.95	96.4	396	0.15	0.59	0.20	0.20	2.95	0.06	0.24	245	83
9H-4, 145-150	77.45	95.5	452	0.19	0.57	0.13	0.25	4.38	0.06	0.19	300	68
12H-4, 145-150	105.95	97.3	448	0.11	0.57	0.11	0.16	5.18	0.05	0.10	570	110
14H-4, 145-150	124.95	122.9	479	0.08	0.35	0.13	0.19	2.69	0.03	0.13	269	100
17H-4, 145-150	144.95	94.9	493	0.20	0.46	0.16	0.30	2.87	0.05	0.13	353	123
19H-4, 145-150	163.95	102.5	478	0.14	0.42	0.21	0.25	2.00	0.04	0.16	262	131
22H-4, 145-150	192.45	89.0	454	0.15	0.49	0.37	0.23	1.32	0.05	0.13	376	284

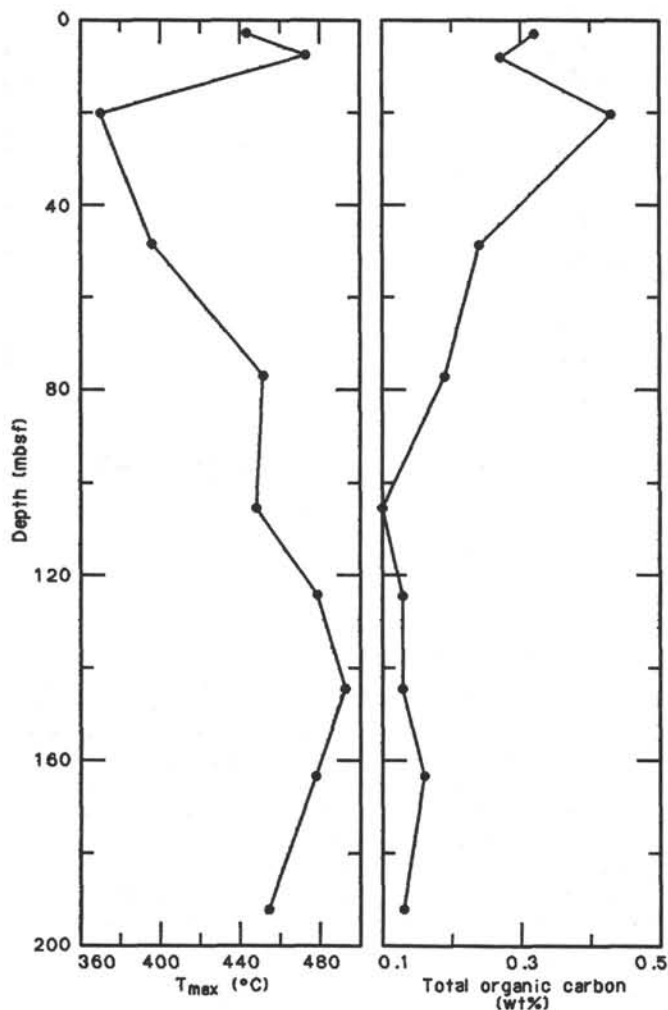


Figure 15. T<sub>max</sub> and total organic carbon for Site 745.

Subunit G2B (80-140 mbsf) is characterized by normal gradients; density and shear strength increase and porosity and water content decrease slightly with depth.

Subunit G2C (140-215 mbsf) is distinguished by a change back to reversed gradients on index-property plots. The vane shear-strength gradient is possibly reversed, and the fall cone

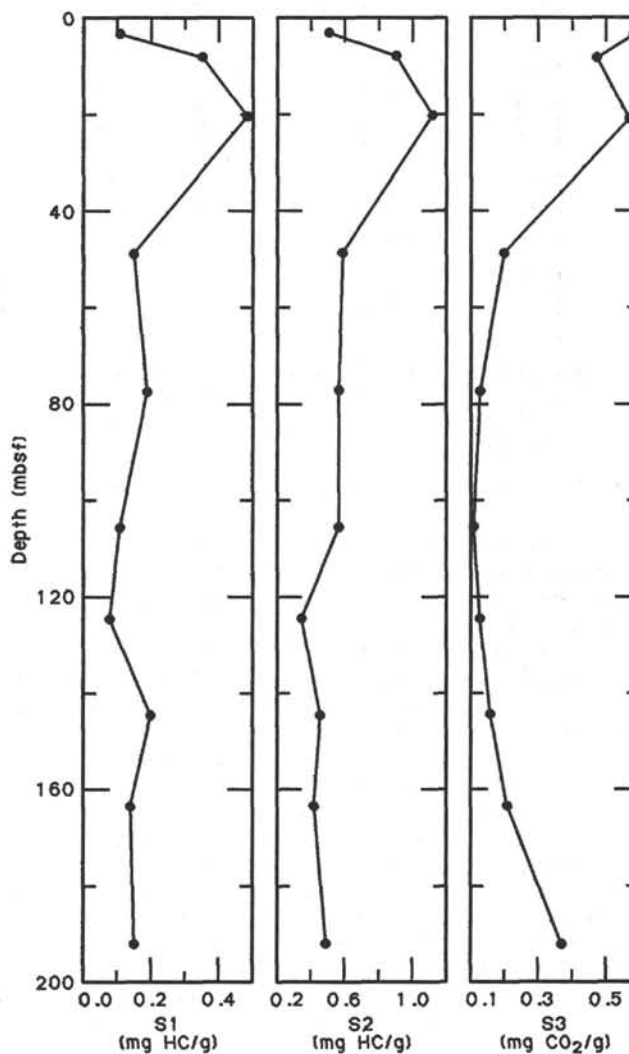


Figure 16. S1, S2, and S3 for Site 745.

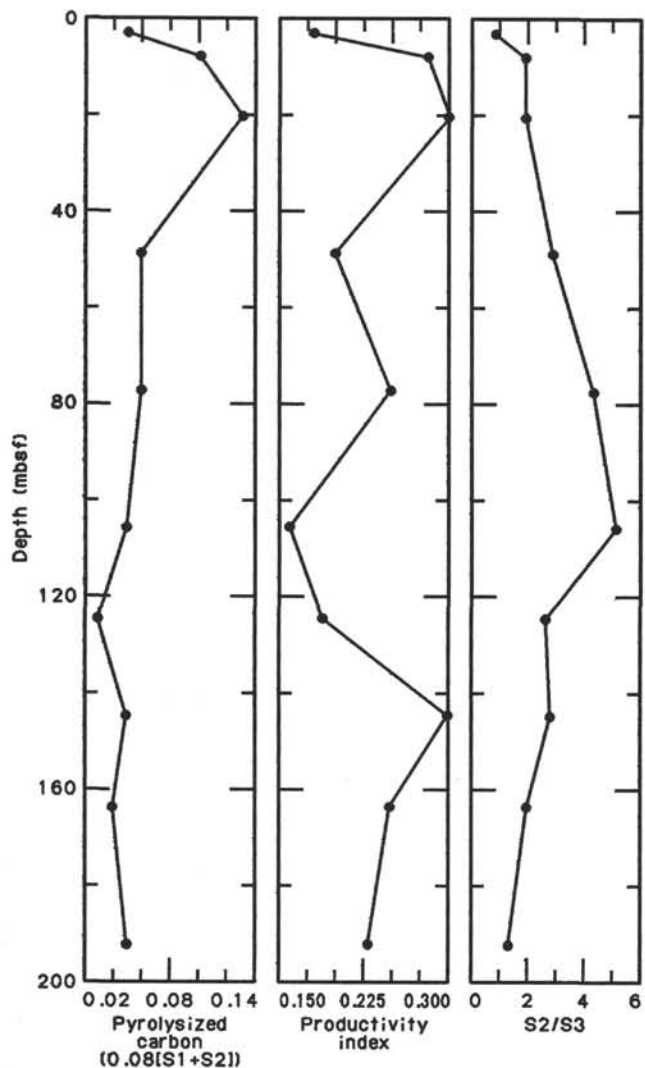


Figure 17. Pyrolyzied carbon, productivity index, and S2/S3, Site 745.

data are somewhat reduced across the interval. The very low values measured by both methods at 179 mbsf may be due to coring disturbance. A very slight trend of decreasing velocity occurs with depth, as well.

Thermal-conductivity values range from 0.6 to 1.1 W/m/°C and average about 0.8 W/m/°C. The few values below 0.59 W/m/°C, the conductivity of water at ambient conditions (Clark, 1966), are considered erroneous.

Temperatures were measured at two sub-bottom depths (91.3 and 177.5 mbsf) in Hole 745B using the Uyeda probe and standard operation procedures (see "Explanatory Notes" chapter). The results are listed in Table 11 and shown graphically for each measurement in Figure 22. Equilibrium temperatures derived from 1/time plots are given in Figure 23. The temperature measurements were not affected by ship surge because seas were calm (<1 m) during the two measurements.

The temperature profile for 91.3 mbsf gives an excellent equilibrium temperature of 6.6°C. The equilibrium temperature was reached only 4 min after penetration, and further disturbances occurred during the 20-min penetration.

The measurement at 177.5 mbsf was made with a slightly different procedure than the other measurements on Leg 119. For this measurement, the probe was latched to the bottom-hole assembly and pushed ahead of the bit, into the sediment under a 4500-kg load. The temperature profile shows only minor dis-

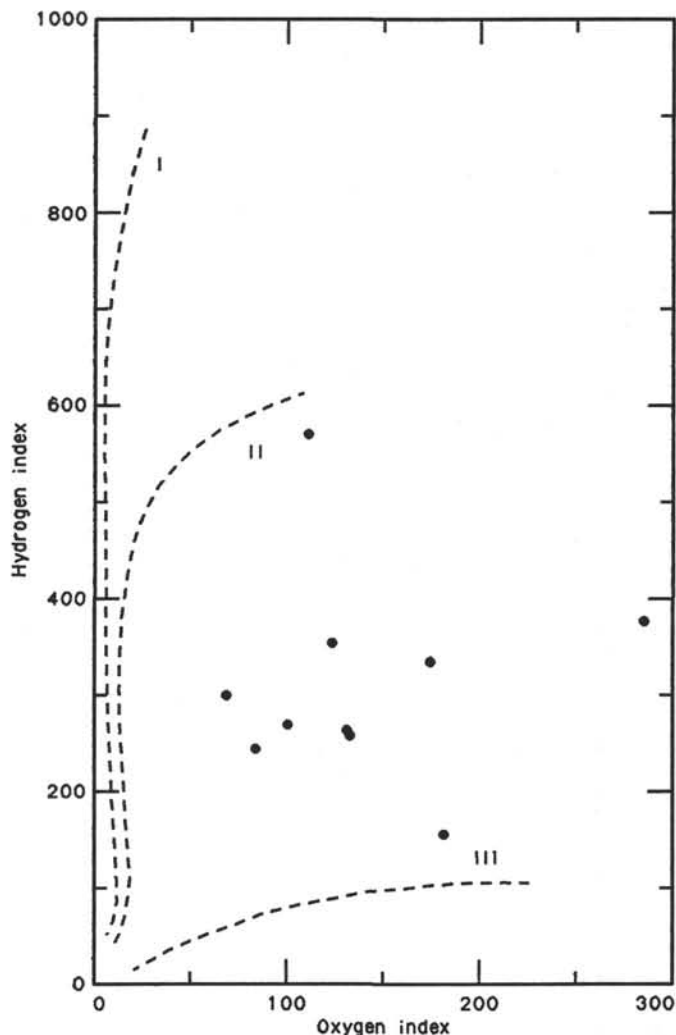


Figure 18. Modified van Krevelen plot of oxygen index vs. hydrogen index, Site 745.

turbances following the initial frictional heating peak; however, a gradual 3°C increase occurs throughout the penetration. This gradual increase, which may reflect further sinking of the probe during the 20-min insertion period, is seen as a continuous increase in the slope of the equilibrium temperature curve. Two estimates of the equilibrium temperature (14.0° and 15.6°C) were made, therefore, to minimize measurement errors caused by possible additional probe insertion.

Temperatures at Site 745 range from 0°C at the seafloor to a temperature gradient of about 83°C/km. The average temperature gradient is not tightly constrained by the three measurements and could vary significantly. The sedimentary section in this interval is composed of silty clay with some diatom layers and has conductivity values averaging about 0.8 W/m/°C. The heat flow, based on these average values for temperature gradient and thermal conductivity, is 66.4 W/m<sup>2</sup> (1.59 HFU).

**Summary**

The sedimentary section drilled at Site 745 is relatively homogenous. This explains the general lack of clearly distinguishable lithologic boundaries in the section. The absence of abrupt changes in geotechnical properties also indicates the absence of significant erosional hiatuses in the section. The section as a whole is typical of sediments in which biogenic silica is the pre-

**Table 8. Wind and weather summary, Sites 745 (59.6°S, 85.9°E) and 746 (54.5°S, 85.9°E).**

Site 745	
8 February, 0800/1500 to 2359 hr	Wind: East-northeast 19 kt. Sea-surface temperature: 1.6°C. Waves: 3–4 m. Sky: Overcast with light snow. Pressure falling rapidly. Air temperature: 1.3°C at 1800 hr.
9 February, 0000 to 2359 hr	Wind: Southeast 28–32 kt; slowly decreasing and shifting to the southwest 18–22 kt throughout the day. Sea-surface temperature: 1.5°–1.8°C. Waves: 5–6 m. Sky: Mostly cloudy to overcast with snow showers in the area. Pressure falling rapidly then increasing rapidly. Air temperature: maximum: 4.6°C at 1200 hr; minimum: 0.2°C at 0000 hr.
10 February, 0000 to 1500 hr	Wind: Southwest to west 20–25 kt decreasing to 12–16 kt by 1200 hr. Sea-surface temperature: 1.6°–2.0°C. Waves: 5–6 m. Sky: Partly cloudy with scattered snow showers in the area. Pressure rising slowly. Air temperature: maximum: 2.9°C at 1200 hr; minimum: 1.1°C at 0000 hr.
Site 746	
10 February, 1500 to 2359 hr	Wind: Shifting to north then northeast and increasing from 8–12 to 15–20 kt. Sea-surface temperature: 2.0°C. Waves: 4 m. Sky: Partly cloudy becoming overcast by 2200 hr; pressure falling. Air temperature: 1.3°C at 1800 hr.
11 February, 0000 to 2359 hr	Wind: East 22–28 kt slowly decreasing to calm by 2000 hr. Sea-surface temperature: 1.6°–1.8°C. Waves: 2–3 m. Sky: Overcast with rain and snow showers mixed. Pressure falling rapidly then steady by 1800 hr. Air temperature: maximum: 2.4°C at 1200 hr; minimum: 1.1°C at 0000 hr.

dominant constituent. These sediments display little response to burial diagenesis (i.e., little consolidation under loads of a few hundred meters of overburden, as evidenced by the absence of well-defined, normal depth gradients and the presence of intervals of significant thickness that exhibit anomalous, reversed depth gradients).

The gradient reversals in the section are possibly due to variations in the relative abundance of biogenic silica and clay (carbonate has a uniform and very low, less than 1%, abundance through out the section at Site 745; see “Organic Geochemistry” section). Zones of relative high clay abundance might act as both permeability barriers and as water retainers from surface and interlayer adsorption, thereby reducing the consolidation (drainage) response to overburden pressure. The relative abundance of clays may also affect silica diagenesis.

### SEISMIC STRATIGRAPHY

Sites 745 and 746 are situated near the crest of a large sedimentary ridge called “East Kerguelen Sedimentary Ridge” by Houtz et al. (1977) and Ramsay and Colwell (1986). The ridge extends for more than 600 km along the foot of the southern Kerguelen Plateau’s steep slope toward the northeast. The ridge is, at the latitude for the Site 745, separated from the about 2000-m-high scarp by channel or moat about 10 km wide with a water depth about 4500 m. The top of the ridge lies in about 4100 m of water and is characterized by wavy topography. The few lines of 3.5-kHz PDR records available indicate wavelengths about 3 km, heights 20–50 m, and crests oriented east-west. The general pattern of the seismic reflectors in the upper 400-m

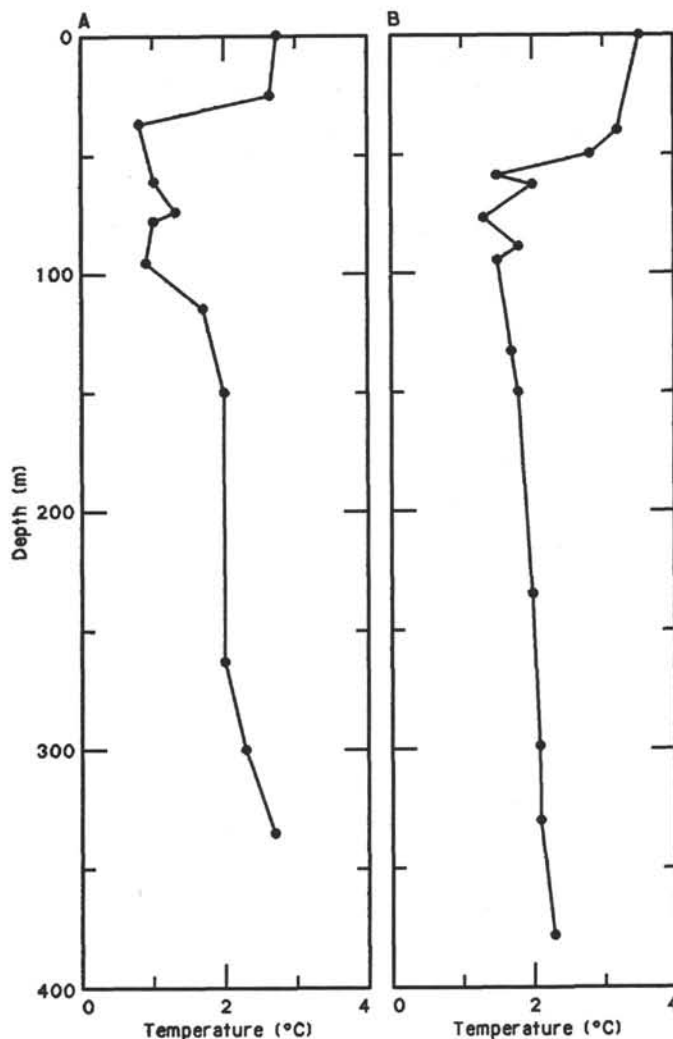


Figure 19. Transcriptions from expendable bathythermograph traces taken in transit after the drill ship left neighboring Site 746. The surface mixed layer was warming and deepening as the ship moved northeast. **A.** 12 February 1988, 1956 hr; 59°31'S, 86°04'E. **B.** 13 February 1988, 0635 hr; 58°01'S, 87°59'E.

two-way traveltime (TWT) of the ridge (see Fig. 24; also Fig. 4, “Site Geophysics” section, this chapter) is wavy and of uniform thickness, indicating predominantly pelagic draping sedimentation. The distribution of reflectors in the uppermost 50–100 m observed on the 3.5-kHz PDR records shows that the thickness and, thus, the accumulation rate of the sequence varies, the rate being greatest on gentle slopes toward the south and much less on slightly steeper slopes. This indicates that currents influence sediment distribution. The deepest reflector on the PDR record (Fig. 25) seems to correspond at Site 745 to an earliest Quaternary age. The configuration of this reflector indicates that deposition of the Quaternary sediments occurs predominantly on the top of the ridge, resulting in the lenticular-shape formation.

The seismic section above the strong reflector near 6 s TWT (Fig. 25) is clearly divided into an upper unit with many well-defined reflections and a lower unit that is almost reflection free. Using a mean sound velocity of 1880 m/s, as determined by the sonobuoy profile, we were able to approximately correlate the stratigraphic sequences identified at Sites 745 and 746 with the seismic profile. Based on this correlation, we inferred that the upper seismic unit approximately corresponds to the combined stratigraphic section penetrated in the two holes and was deposited in late Miocene to Quaternary time.

**Table 9. Diatom species from daily collections off the stern of the drill ship in a 20- $\mu$ m-mesh net with a diameter of 10 cm. Although samples collected at the surface are commonly photoinhibited and bleached, the diversity in this listing is for comparison with the assemblage in the sediments.**

---

*Amphiprora* sp.  
*Asteromphalus hookeri*  
*A. hyalinus*  
*A. parvulus*  
*Chaetoceros atlanticus*  
*C. bulbosus*  
*C. castracanei*  
*C. convolutus*  
*C. curvisetus*  
*C. dictyeta*  
*C. sp. cf. dictyeta*  
*C. flexuosus*  
*C. neglectus* (with resting spores)  
*C. pendulus*  
*C. peruvianus*  
*Corethron criophilum*  
*C. inerme*  
<sup>a</sup>*Dactyliosolen antarcticus*  
*D. tenuijunctus*  
*Eucampia antarctica*  
<sup>a</sup>(winter stage formation in southern form)  
 (northern form present in small numbers!)  
<sup>a</sup>*Navicula directa*  
<sup>a</sup>*Nitzschia angulata*  
*N. closterium*  
<sup>a</sup>*N. curta*  
<sup>a</sup>*N. cylindrus*  
*N. inflatula?*  
<sup>a</sup>*N. kerguelensis*  
*N. lecointei?*  
*N. lineola?*  
*N. prolongatoides*  
*N. ritscheri*  
<sup>a</sup>*N. separanda*  
*N. subcurvata*  
*N. spp.* (ribbon colonies)  
*N. spp.* (colonies of needlelike cells with overlapping tips)  
*Rhizosolenia alata*  
*R. chunii*  
*R. cylindrus*  
*R. hebetata* f. *semispina*  
*R. simplex*  
<sup>a</sup>*Synedra reinboldii*  
<sup>a</sup>*Thalassiosira ambigua?*  
*T. frenguelli*  
<sup>a</sup>*T. gracilis*  
*T. sp. cf. graviora*  
<sup>a</sup>*T. lentiginosa*  
<sup>a</sup>*T. oliverana*  
*T. perpusilla*  
*T. ritscheri*  
 (heavy and light silicification)  
<sup>a</sup>*T. trifluta*  
*T. tumida*, northern variety  
<sup>a</sup>(heavy and light silicification)  
*Tropidoneis glacialis*  
<sup>a</sup>*Synedra reinboldii*

---

<sup>a</sup> Also found in surface sediments and Sample 119-745B-1H-1, 0 cm (mud line).

The two seismic units above the strong reflector at 6.06 s TWT (see "Site Geophysics" section) appear to be truncated by the channel on the southeastern side of the ridge. Erosion in the uppermost layers of the ridge sediments is also indicated on the eastern side of the ridge, near the turning point for the profile (see Fig. 1, "Site Geophysics" section). Consequently, late Miocene age and younger layers seem to be truncated by the channel, indicating the occurrence of currents sufficient to cause erosion or cause preferential sedimentation on the sedimentary ridge. Erosion may still be active. The erosion may be connected with a local intensification of the northward flow of cool Ant-

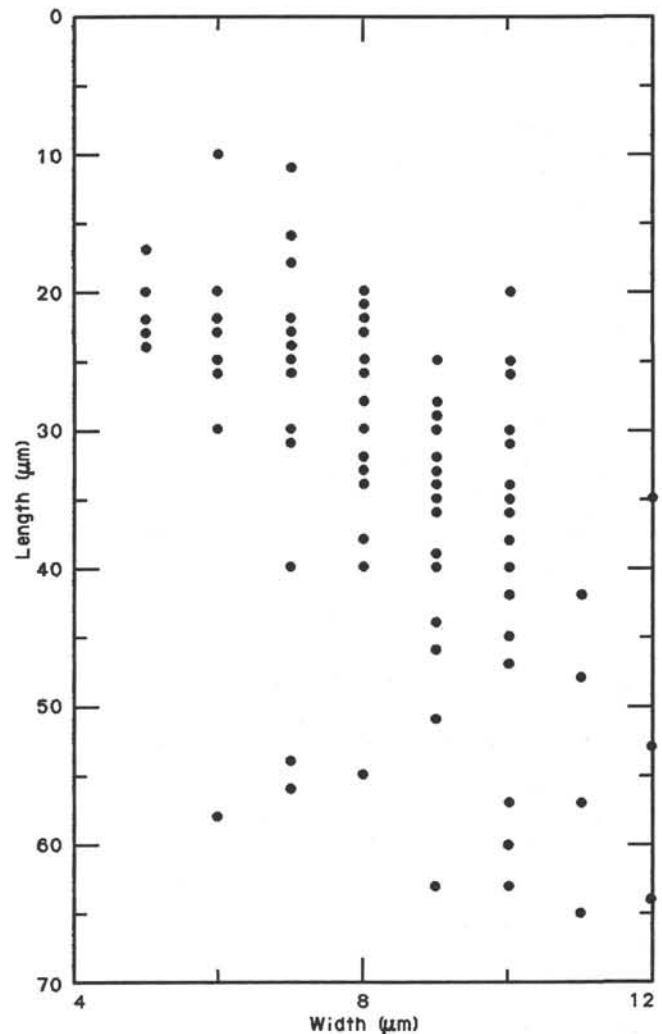


Figure 20. *Nitzschia kerguelensis* measured microscopically aboard ship at 1000 $\times$  from a Hyrax mount of mud-line Sample 119-745B-1H-1, 0 cm. The first 100 valves found that were entire and lying flat were measured. This procedure may have been selective for smaller valves that may be less likely to be broken, as many fragments were in the sample.

arctic Bottom Water along the slope of the southern Kerguelen Ridge.

Hypothetically, this bottom current may carry fine-grained terrigenous particles from the shelf of Antarctica. This process may be increased considerably in periods when the melting of ice at the Antarctic shelf break supplies fine glacial debris directly to the continental slope and deep water, while the clay is trapped in the shelf depressions in periods with less extensive ice sheets. This could offer an explanation for the variable clay content observed in the pelagic sequences at the site.

## SUMMARY AND CONCLUSIONS

Site 745 is located near the crest of a large sedimentary ridge, the "East Kerguelen Sedimentary Ridge" of Houtz et al. (1977), which extends for more than 600 km toward the northeast along the steep eastern slope of the southern Kerguelen Plateau. The site lies beneath present-day Antarctic Bottom Water, and seismic stratigraphy indicates that currents have influenced sediment distribution.

The 215-m-thick section of silty diatom ooze and diatom clay cored at Site 745 (Hole 745B) is of mixed biosiliceous pelagic-

Table 10. Physical properties measured at Site 745.

Core, section, interval (cm)	Depth (mbsf)	Water content (%)	Porosity (%)	Wet-bulk density (g/cm <sup>3</sup> )	Dry-bulk density (g/cm <sup>3</sup> )	Grain density (g/cm <sup>3</sup> )	Undrained shear strength		Compressional- wave velocity (m/s)	Thermal conductivity (W/m/°C)	Temperature drift rate (°C/min)
							Vane (kPa)	Fall cone (kPa)			
119-745A-											
1H-1, 113	1.63								1500.5		
1H-1, 114	1.64	63.82	82.49	1.37	0.50	2.68		3.6			
1H-1, 118	1.68						3.7				
1H-2, 39	2.39	58.42	77.40	1.39	0.58	2.45			1460.6		
1H-2, 40	2.40							3.3			
1H-2, 42	2.42						7.2				
1H-2, 70	2.70									0.853	0.074
1H-3, 62	4.12	57.27	78.82	1.48	0.63	2.80		13.0	1465.3		
1H-3, 66	4.16						6.4				
1H-4, 70	5.70									0.717	0.009
1H-5, 90	7.40	72.24	83.95	1.27	0.35	1.99	13.4	16.0	1489.3		
1H-5, 92	7.42									0.727	0.028
1H-6, 70	8.70										
1H-7, 41	9.91						10.8				
1H-7, 44	9.94	69.96	85.10	1.28	0.38	2.45		14.0	1510.8		
1H-7, 50	10.00									0.778	0.030
119-745B-											
1H-1, 121	1.21							4.8	1474.2		
1H-1, 122	1.22	66.84	82.36	1.29	0.43	2.32					
1H-1, 124	1.24						4.8				
1H-2, 68	2.18						4.1				
1H-2, 69	2.19	67.61	84.47	1.31	0.42	2.61				0.715	0.067
1H-2, 70	2.20										
1H-2, 71	2.21							4.9			
1H-2, 73	2.23								1460.3		
1H-3, 70	3.70									0.810	0.038
1H-3, 138	4.38								1459.2		
1H-3, 140	4.40	66.45	82.72	1.34	0.45	2.42	7.4				
1H-4, 30	4.80									0.881	0.049
2H-1, 70	5.70									0.620	0.052
2H-1, 100	6.00	69.08	82.87	1.32	0.41	2.16	6.8	4.2	1505.1		
2H-3, 70	8.70									0.775	0.028
2H-4, 94	10.44	71.95	87.11	1.29	0.36	2.63	3.7	7.7	1556.1		
2H-5, 70	11.70									0.749	0.039
2H-7, 16	14.16	67.24	82.56	1.35	0.44	2.30	4.6	9.0	1541.3		
2H-7, 40	14.40									0.883	0.035
3H-1, 88	15.38	70.30	84.11	1.31	0.39	2.23	9.1	17.0	1511.4		
3H-3, 90	18.40	74.26	86.20	1.25	0.32	2.14	3.7	8.1	1528.1		
3H-5, 80	21.30	68.72	83.55	1.33	0.41	2.31	7.4	21.0	1536.6		
4H-1, 70	24.70									0.726	0.069
4H-2, 86	26.36	60.51	78.09	1.39	0.55	2.33	17.2	34.0	1483.9		
4H-3, 70	27.70									0.944	0.036
4H-4, 112	29.62	68.58	81.13	1.28	0.40	1.96		39.0	1527.8		
4H-5, 70	30.70									0.705	0.029
4H-7, 30	33.30	58.21	77.72	1.48	0.62	2.52	6.0	8.1	1497.8		
4H-7, 40	33.40									0.931	0.034
5H-2, 70	35.70									0.559	-0.019
5H-2, 100	36.00	67.66	83.10	1.28	0.42	2.35	12.8	21.0	1500.0		
5H-4, 70	38.70									0.945	0.008
5H-4, 128	39.28	56.28	76.10	1.44	0.63	2.49	17.8	24.0	1532.7		
5H-6, 70	41.70									0.760	-0.015
5H-6, 80	41.80	61.41	79.01	1.35	0.52	2.37	22.8	27.0	1570.0		
5H-7, 40	42.90									0.960	0.011
6H-2, 70	45.20									0.957	0.096
6H-2, 99	45.49	53.61	75.10	1.54	0.71	2.63	17.8	30.0	1476.4		
6H-4, 45	47.95	51.09	75.33	1.61	0.79	2.95	25.0	62.0	1504.8		
6H-4, 70	48.20									0.941	0.041
6H-6, 70	51.20									0.940	0.048
6H-6, 90	51.40	51.81	75.54	1.56	0.75	2.90	21.5	62.0	1511.6		
7H-1, 70	53.20									0.810	0.026
7H-1, 82	53.32	56.48	75.93	1.44	0.63	2.45	18.2	34.0		1.008	0.022
7H-3, 70	56.20										
7H-3, 107	56.57	55.90	75.40	1.49	0.66	2.43	21.3	24.0			
7H-4, 82	57.82								1519.4		
7H-5, 70	59.20									0.907	0.022
7H-5, 120	59.70	61.53	80.18	1.39	0.54	2.54	20.3	39.0	1576.9		
7H-7, 40	61.90									1.048	0.023
8H-1, 90	62.90	65.01	82.80	1.38	0.48	2.60	19.7	35.0	1511.7		
8H-2, 70	64.20									0.740	0.058
8H-3, 70	65.70									0.822	0.030
8H-3, 72	65.72	65.10	81.33	1.43	0.50	2.34	21.3	39.0	1589.1		
8H-5, 70	68.70	62.34	80.61	1.37	0.52	2.52	21.3	44.0	1518.9		
8H-6, 70	70.20									0.850	0.043

Table 10 (continued).

Core, section, interval (cm)	Depth (mbsf)	Water content (%)	Porosity (%)	Wet-bulk density (g/cm <sup>3</sup> )	Dry-bulk density (g/cm <sup>3</sup> )	Grain density (g/cm <sup>3</sup> )	Undrained shear strength		Compressional- wave velocity (m/s)	Thermal conductivity (W/m/°C)	Temperature drift rate (°C/min)
							Vane (kPa)	Fall cone (kPa)			
8H-7, 15	71.15	63.62	79.78	1.39	0.51	2.26	19.5	39.0			
8H-7, 52	71.52								1523.6		
9H-1, 70	72.20						21.7			0.796	0.074
9H-1, 71	72.21	64.77	79.98	1.30	0.46	2.17					
9H-1, 72	72.22							42.0	1500.0		
9H-2, 65	73.65	55.12	74.04	1.42	0.64	2.34		43.0			
9H-2, 66	73.66								1546.8		
9H-2, 67	73.67						34.9				
9H-3, 69	75.19	54.91	75.97	1.47	0.66	2.62					
9H-3, 70	75.20									0.811	0.033
9H-4, 67	76.67						43.1				
9H-4, 71	76.71							40.0	1481.4		
9H-6, 68	79.68	69.93	83.85	1.24	0.37	2.22		42.0	1502.9		
9H-6, 70	79.70						36.4			0.949	0.039
10H-1, 70	81.70									0.832	0.073
10H-1, 97	81.97						34.2				
10H-1, 99	81.99	63.06	79.13	1.32	0.49	2.22					
10H-1, 100	82.00							39.0	1516.1		
10H-3, 70	84.70									0.990	0.034
10H-3, 86	84.86	55.30	75.39	1.43	0.64	2.49		40.0	1504.2		
10H-3, 89	84.89						36.4				
10H-5, 64	87.64	56.25	74.90	1.43	0.62	2.33		58.0	1522.6		
10H-5, 66	87.66						53.5				
10H-5, 70	87.70									0.830	0.037
10H-7, 40	90.40	52.24	71.16	1.46	0.70	2.27				0.937	0.032
10H-7, 42	90.42								1507.0		
11H-2, 49	92.49	59.27	77.19	1.37	0.56	2.33					
11H-2, 50	92.50								1513.3		
11H-2, 53	92.53							37.0			
11H-2, 54	92.54						32.7				
11H-2, 70	92.70									0.840	0.070
11H-4, 64	95.64						31.9				
11H-4, 66	95.66	64.67	79.53	1.30	0.46	2.12					
11H-4, 67	95.67							37.0	1529.7		
11H-4, 70	95.70									0.814	0.040
11H-5, 52	97.02								1514.2		
11H-5, 57	97.07	51.66	70.57	1.45	0.70	2.26		65.0			
11H-5, 60	97.10						67.6				
11H-6, 70	98.70									0.977	0.048
11H-7, 20	99.70	53.39	75.10	1.45	0.68	2.66					
11H-7, 23	99.73								1511.7		
12H-1, 87	100.87	58.94	78.31	1.39	0.57	2.53					
12H-1, 88	100.88							53.0	1521.9		
12H-1, 90	100.90						59.4				
12H-2, 70	102.20									0.948	0.102
12H-3, 62	103.62	46.26	69.76	1.58	0.85	2.71					
12H-3, 65	103.65						65.3				
12H-3, 67	103.67							80.0	1515.0		
12H-4, 70	105.20									0.903	0.045
12H-5, 63	106.63						62.4				
12H-5, 65	106.65	53.48	74.76	1.50	0.70	2.60					
12H-5, 66	106.66							65.0	1509.0		
12H-6, 70	108.20									0.994	0.057
12H-7, 12	109.12						73.5				
12H-7, 13	109.13	45.81	68.45	1.59	0.86	2.59					
12H-7, 15	109.15							85.0	1523.6		
12H-7, 40	109.40									1.073	0.036
13H-1, 70	110.20									1.043	0.074
13H-1, 77	110.27								1558.9		
13H-1, 83	110.33	46.00	67.37	1.57	0.85	2.45					
13H-1, 85	110.35										
13H-1, 87	110.37						67.3				
13H-3, 70	113.20									0.939	0.027
13H-4, 88	114.88	50.42	70.89	1.49	0.74	2.41		71.0			
13H-4, 92	114.92						78.9				
13H-5, 70	116.20									0.903	0.005
13H-6, 6	117.06	49.52	69.83	1.51	0.76	2.38		75.0	1531.8		
13H-6, 9	117.09						63.8				
13H-7, 40	118.90									1.052	0.046
14H-1, 57	119.57								1503.6		
14H-1, 58	119.58							84.0			
14H-1, 59	119.59	50.01	71.16	1.49	0.74	2.49					
14H-1, 61	119.61						74.2				
14H-1, 70	119.70									0.096	0.078
14H-1, 70	122.70						69.6				
14H-3, 71	122.71	46.66	68.06	1.63	0.87	2.46					

Table 10 (continued).

Core, section, interval (cm)	Depth (mbsf)	Water content (%)	Porosity (%)	Wet-bulk density (g/cm <sup>3</sup> )	Dry-bulk density (g/cm <sup>3</sup> )	Grain density (g/cm <sup>3</sup> )	Undrained shear strength		Compressional- wave velocity (m/s)	Thermal conductivity (W/m/°C)	Temperature drift rate (°C/min)
							Vane (kPa)	Fall cone (kPa)			
14H-3, 72	122.72							89.0			
14H-3, 75	122.75								1531.0		
14H-3, 70	122.70									0.994	0.049
14H-5, 67	125.67						93.9			1.055	0.059
14H-5, 70	125.70	48.52	70.49	1.58	0.81	2.56					
14H-5, 71	125.71							103.0			
14H-5, 75	125.75								1529.4		
14H-7, 40	128.40									1.088	0.033
15H-1, 70	129.20									0.821	0.052
15H-1, 102	129.52								1511.6		
15H-1, 104	129.54							80.0			
15H-1, 106	129.56						73.1				
15H-2, 70	130.70									0.915	0.038
15H-3, 68	132.18						83.5				
15H-3, 71	132.21								1534.7		
15H-3, 72	132.22	57.45	76.98	1.42	0.60	2.49					
15H-3, 73	132.23							71.0			
15H-4, 70	133.70									0.950	0.060
15H-5, 45	134.95	51.55	71.87	1.49	0.72	2.42					
15H-5, 49	134.99							63.0			
15H-5, 50	135.00								1535.5		
15H-5, 52	135.02						73.1				
15H-6, 87	136.87							34.0			
15H-6, 88	136.88	61.30	79.11	1.37	0.53	2.40					
15H-6, 90	136.90						39.4		1525.6		
17H-1, 70	139.70									0.695	0.057
17H-2, 110	141.60	60.95	80.55	1.37	0.54	2.67	62.6	85.0	1605.9		
17H-3, 70	142.70									0.914	0.027
17H-4, 90	144.40	49.39	71.60	1.61	0.81	2.61	66.1	69.0	1565.6		
17H-5, 70	145.70									1.030	0.048
17H-6, 65	147.15	50.55	74.31	1.56	0.77	2.86	88.1	82.0	1548.4		
17H-7, 40	148.40									0.902	0.036
18H-2, 86	150.86	49.94	71.83	1.51	0.76	2.58	95.1	103.0			
18H-4, 70	153.70									0.859	0.037
18H-5, 98	155.48	54.80	76.56	1.52	0.69	2.72	83.5	71.0	1556.0		
18H-6, 70	156.70									0.906	0.042
18H-7, 35	157.85	54.35	74.07	1.47	0.67	2.42	100.9	123.0	1574.2		
19H-2, 115	160.65	50.93	71.40	1.46	0.72	2.43	78.9	80.0	1515.7		
19H-4, 70	163.20									1.010	0.042
19H-6, 70	166.20									0.968	0.050
19H-7, 50	167.50	47.76	70.87	1.61	0.84	2.69	82.3	103.0			
20H-2, 80	169.80	47.00	68.51	1.54	0.81	2.48	42.9	174.0	1565.6		
20H-3, 70	171.20									0.982	0.041
20H-4, 82	172.82						68.4	123.0	1575.3		
20H-5, 70	174.20									0.967	0.053
20H-7, 30	176.80	49.66	72.69	1.57	0.79	2.72	97.4	123.0	1510.7		
21H-2, 80	179.30	52.98	74.20	1.52	0.72	2.57	11.6	21.0	1530.2		
21H-4, 70	182.20									1.002	0.046
21H-6, 70	185.20									1.002	0.055
21H-7, 40	186.40	52.71	73.47	1.54	0.73	2.50		74.0	1559.2		
22H-2, 9	188.09							88.0			
22H-2, 90	188.90	50.30	70.55	1.56	0.78	2.39			1547.1		
22H-3, 70	190.20									0.896	0.029
22H-4, 80	191.80	54.65	74.57	1.49	0.67	2.45		74.0	1553.6		
22H-5, 70	193.20									0.664	-0.038
22H-7, 5	195.55	51.52	74.20	1.56	0.75	2.73		88.0	1572.0		
23H-1, 70	196.70								1540.2		
23H-1, 71	196.71									98.0	
23H-1, 73	196.73	55.16	75.88	1.46	0.65	2.58					
23H-1, 75	196.75						77.7				
23H-3, 70	199.70									0.842	0.024
23H-3, 94	199.94						76.5				
23H-3, 97	199.97	54.27	73.06	1.44	0.66	2.30					
23H-3, 98	199.98							96.0			
23H-3, 99	199.99								1541.8		
23H-5, 70	202.70									0.935	0.049
23H-5, 80	202.80						122.9				
23H-5, 81	202.81	52.24	70.67	1.44	0.69	2.22					
23H-5, 82	202.82							140.0			
23H-5, 83	202.83								1549.3		
23H-7, 53	205.53	53.36	72.59	1.45	0.68	2.33					
23H-7, 57	205.57								1546.8		
24H-1, 83	206.33	52.94	72.89	1.46	0.68	2.41					
24H-1, 84	206.34						81.2				
24H-1, 86	206.36									89.0	
24H-1, 88	206.38								1550.2		

Table 10 (continued).

Core, section, interval (cm)	Depth (mbsf)	Water content (%)	Porosity (%)	Wet-bulk density (g/cm <sup>3</sup> )	Dry-bulk density (g/cm <sup>3</sup> )	Grain density (g/cm <sup>3</sup> )	Undrained shear strength		Compressional- wave velocity (m/s)	Thermal conductivity (W/m/°C)	Temperature drift rate (°C/min)
							Vane (kPa)	Fall cone (kPa)			
24H-3, 84	209.34						89.3				
24H-3, 85	209.35	52.30	71.41	1.45	0.69	2.29					
24H-3, 87	209.37								1527.5		
24H-3, 88	209.38										
24H-4, 23	211.73								145.0		
24H-5, 24	211.74	59.88	78.24	1.40	0.56	2.42			170.0		1536.8
24H-5, 27	211.77										
24H-7, 17	214.67								136.8		
24H-7, 18	214.68	53.18	73.47	1.46	0.68	2.46			121.8		
24H-7, 20	214.70								150.0		1538.8

terigenous character, with practically no carbonate accumulation. Foraminifers and calcareous nannofossils occur in only a few samples and are strongly etched because of deposition near the CCD. Abundant to common, well-preserved diatom and radiolarian assemblages are present throughout the section, and, together with an excellent magnetostratigraphy, they indicate that a complete uppermost Miocene to Quaternary section was recovered at the site. The Quaternary/Pliocene boundary lies at about 85 mbsf, the lower/upper Pliocene boundary at about 135 mbsf, and the Miocene/Pliocene boundary at about 206 mbsf in Hole 745B. The uppermost Miocene (5.3–5.7 Ma) is characterized by the presence of low-latitude diatoms of the genera *Thalassiosira* and *Nitzschia*, which were also found in the uppermost Miocene of Sites 737, 738, and 744. Within the Quaternary section, abundance fluctuations of the radiolarian *Theocalyptra davisiana* and the diatom *Eucampia antarctica* indicate the possibility that glacial-interglacial cycles can be recognized. Preliminary study indicates that the more clay-rich intervals of the Quaternary probably correspond to the glacials.

A single lithologic unit with two subunits is recognized at Site 745. Subunit IA (0–37 mbsf) is dominated by diatom ooze with 70%–90% diatoms, with sporadic minor amounts of quartz-feldspar silt, radiolarians, or clay. Subunit IB (37–215 mbsf) is characterized by more clearly alternating intervals of diatom ooze and diatomaceous clay on a scale of decimeters to a few meters. The clay-rich horizons of this subunit contain <50% diatoms, and the silt content of the subunit is also significant, reaching a maximum of 35%. Minor thin claystone, silt, and volcanic ash layers are also present in Subunit IB. Abundance estimations from smear slides for diatoms and clay in Subunit IB reveal a clear inverse relationship, indicating that either pelagic sedimentation occurred at a steady rate and clay sedimentation was variable or the converse. The origin of the clay fraction is uncertain, but some of it was probably ice rafted, especially in the upper 70 m of Hole 745B, where a more obviously ice-rafted quartz-silt component follows a roughly similar trend of alternation with the diatom ooze. Although bioturbation is evident in parts of the section cored at Site 745, it is generally diffuse, except in the upper cores, where some distinct burrows are present.

A significant feature of Site 745 is the presence throughout most of the cored sedimentary section of dispersed limestones, granules, and small pebbles originating from a metamorphic basement source area. Small pebbles of quartz-feldspar biotite gneiss, amphibolite, and granite, some of which resemble the clasts found in Prydz Bay glacial sediments, are clearly ice rafted. No continental basement that could supply such clasts lies nearer than the Antarctic margin. Similarly, the freshness of the grains and their angular to subangular shapes indicate that much of the quartz-feldspar silt fraction present in the Site 745

sediments is also ice rafted. Broad, complex peaks of ice-rafted material occur between 0 and 70 mbsf (0–1.2 Ma) and between 145 and 195 mbsf (4.0–about 5.0 Ma), indicating enhanced glaciation in the late Quaternary and early Pliocene. However, at least some ice rafting continued throughout the remainder of the Quaternary and Pliocene and latest Miocene.

The section cored at Site 745, as a whole, is typical of sediments in which biogenic silica is the predominant constituent; namely they display little response to burial diagenesis (i.e., they show little consolidation under the load of a few hundred meters of overburden). Two geotechnical units are recognized that correspond roughly to the two lithologic units. Geotechnical unit G1 (0–45 mbsf) is a diatom ooze with physical-property profiles that exhibit little overall change in character or gradient with depth, although some small-scale variation is present. Geotechnical unit G2 (45–210 mbsf) is a diatomaceous silty clay, the upper contact of which displays a change in the gradients on physical-property profiles, especially on the density plot. The absence of abrupt changes in geotechnical properties indicates the absence of significant erosional hiatuses in Hole 745B.

Total organic carbon is low (0.3%–0.4%) in the upper 20 m of Hole 745B and decreases to values of 0.1% by a depth of 100 mbsf, where it remains to the bottom of the hole. The most intense zone of bacterial activity occurs between 3 and 49 mbsf based on downhole ammonium and phosphate concentrations, and pH, alkalinity, and sulfate analyses indicate that only a small amount of reactable organic matter is being incorporated into the sediments. Kerogen is of mixed marine and terrestrial origin.

Seismic stratigraphy reveals that the late Miocene age and younger sediments cored at Site 745 are truncated to the southeast by a channel, indicating the influence of bottom currents on erosion and preferential sedimentation. The bottom currents originating below the slope of the Antarctic margin may carry fine-grained terrigenous materials, which have been swept off the Antarctic shelf, northward to Site 745. Such transport may have been increased during glacial periods when the melting of ice at the Antarctic shelf break supplied fine glacial debris directly onto the continental slope. Thus, enhanced terrigenous transport to Site 745 would occur during glacial intervals. Alternatively, some of the non-ice-rafted detrital clays at Site 745 may have been supplied from the shallow northern Kerguelen Plateau, because reworked diatoms and radiolarians of various ages occur throughout the Hole 745B sediments, as do benthic diatoms that are derived from environments within the photic zone (about 0–100 m).

#### REFERENCES

- Berggren, W. A., Kent, D. V., Flynn, J. J., and Van Couvering, J. A., 1985. Cenozoic geochronology. *Geol. Soc. Am. Bull.*, 96:1407–1418.

- Clark, S. P., 1966. Handbook of physical constants. *Geol. Soc. Am. Mem.*, 97.
- Deroo, G., Herbin, J. P., Roucache, J. R., and Tissot, B., 1979. Organic geochemistry of Cretaceous mudstones and marly limestones from DSDP Sites 400 and 402, Leg 48, eastern North Atlantic. In Montadert, L., Roberts, D. G., et al., *Init. Repts. DSDP*, 48: Washington (U.S. Govt. Printing Office), 921-930.
- Deroo, G., Herbin, J. P., Roucache, J. R., Tissot, B., Albrecht, P., and Dastillung, M., 1978. Organic geochemistry of some Cretaceous claystones from Site 391, Leg 44, western North Atlantic. In Benson, W. E., Sheridan, R. E., et al., *Init. Repts. DSDP*, 44: Washington (U.S. Govt. Printing Office), 593-598.
- Eldholm, O., Thiede, J., et al., 1987. *Proc. ODP, Init. Repts.*, 104: College Station, TX (Ocean Drilling Program).
- Gieskes, J. M., 1983. The chemistry of interstitial waters of deep sea sediments: interpretation of deep sea drilling data. In Riley, J. P., and Chester, R. (Eds.), *Chemical Oceanography* (vol. 8): New York (Academic Press), 221-269.
- Houtz, R. E., Hayes, D. E., and Markl, R. G., 1977. Kerguelen Plateau bathymetry, sediment distribution and crustal structure. *Mar. Geol.*, 25:95-130.
- McDuff, R. E., 1978. Conservative behavior of calcium and magnesium in interstitial waters of marine sediments: identification and interpretation [Ph.D. dissert.]. Univ. of California, San Diego.
- McDuff, R. E., and Geiskes, J. M., 1976. Calcium and magnesium profiles in DSDP interstitial waters: diffusion or reaction? *Earth Planet. Sci. Lett.*, 33:1-10.
- Ramsay, D. C., and Colwell, J. B., 1986. *Rig Seismic* research cruise 2: Kerguelen Plateau, southern Indian Ocean, initial report. *Rept. Bur. Min. Resour., Geol. Geophys. (Aust.)*, 270:1-41.
- Stumm, W., and Morgan, J. J., 1981. *Aquatic Chemistry* (2nd ed.): New York (Wiley).
- Tissot, B. P., and Welte, D. H., 1984. *Petroleum Formation and Occurrence* (2nd ed.): Berlin (Springer-Verlag).

Ms 119A-113

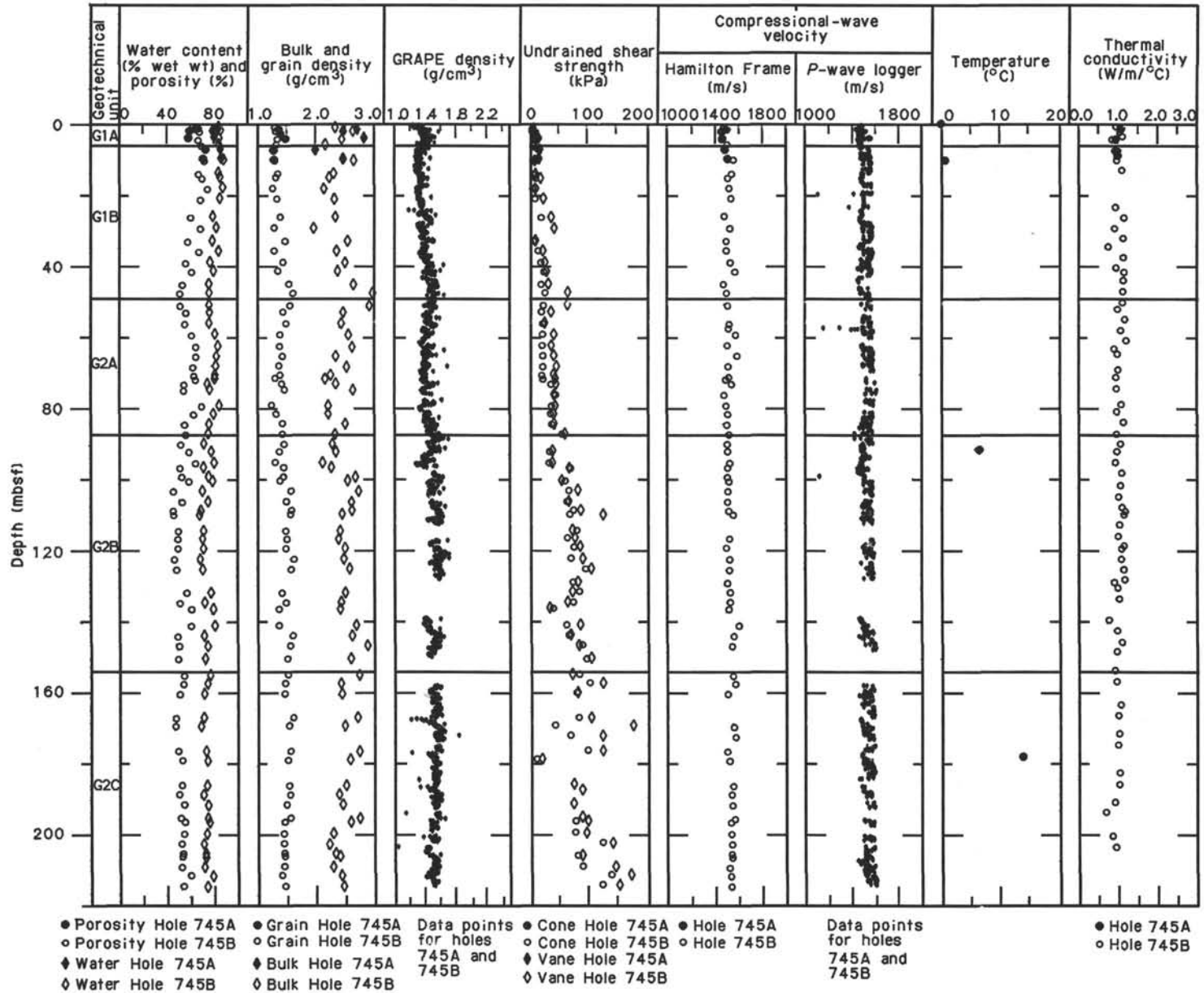


Figure 21. Physical properties measured at Site 745.

Table 11. Temperature measurements, Hole 745B.

Depth (mbsf)	Core no.	Time (min)			Temperature (°C)		
		IB	ET	ML	T <sub>SF</sub>	T <sub>M</sub>	T <sub>B</sub>
91.3	10H	23	23	8	0.0	0.7	6.5
177.5	20H	20	20	5	0.1	<sup>a</sup> 0.5	13.7

Note: IB = probe in sediment; ET = probe equilibration time; ML = probe at "mud line" (actually 10 mbsf); T<sub>SF</sub> = coldest temperature immediately prior to probe penetration; T<sub>M</sub> = temperature at 10 mbsf; T<sub>B</sub> = equilibration temperature in sediment.

<sup>a</sup> Temperature at 0 mbsf because a shorter assembly was used to hold the probe in place (and push it into the bottom with 10,000-lb force).

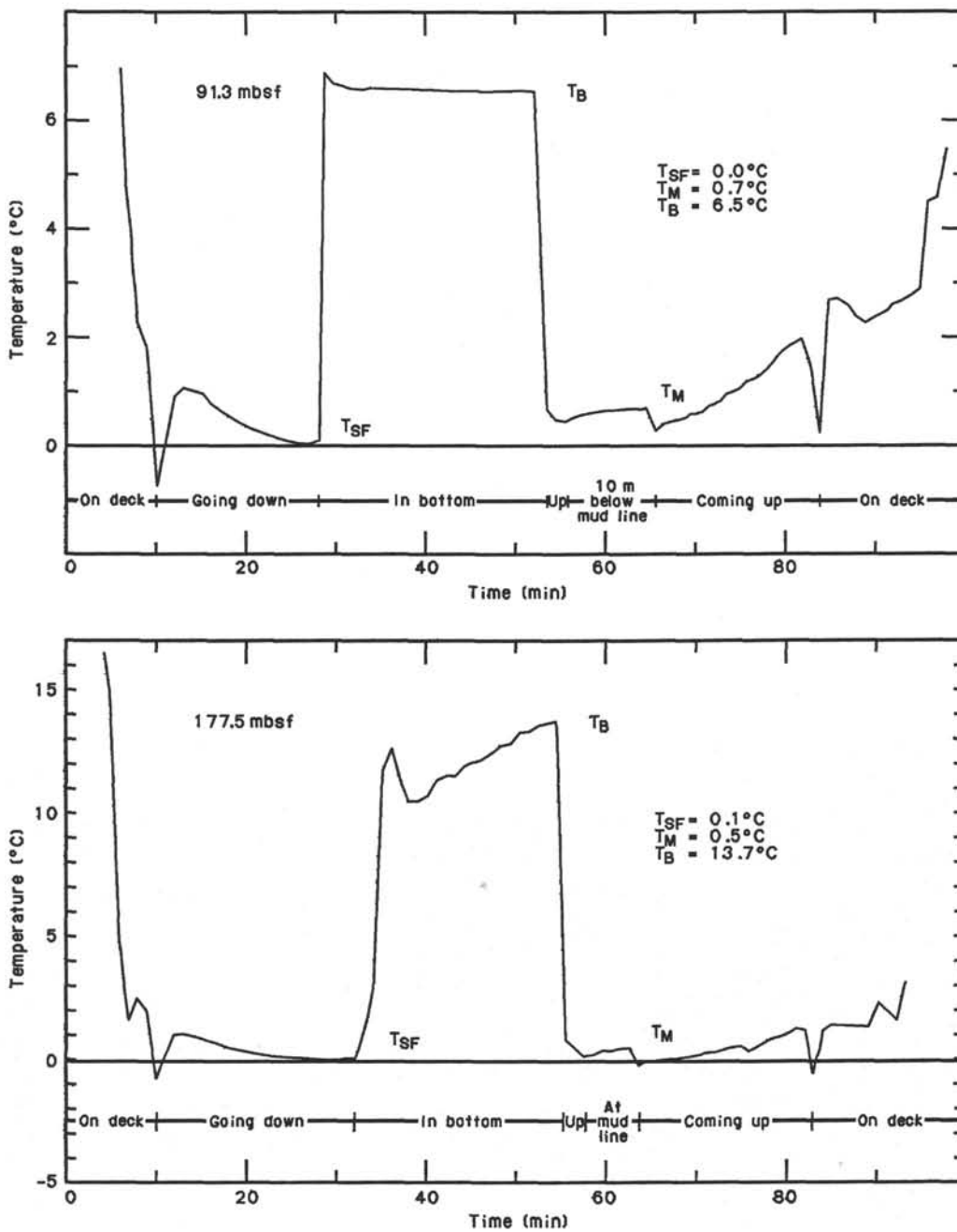


Figure 22. Temperature vs. measurement time for the two Uyeda probe deployments in Hole 745B (see Table 11 for explanation of critical temperature points T<sub>SF</sub>, T<sub>M</sub>, and T<sub>B</sub>).

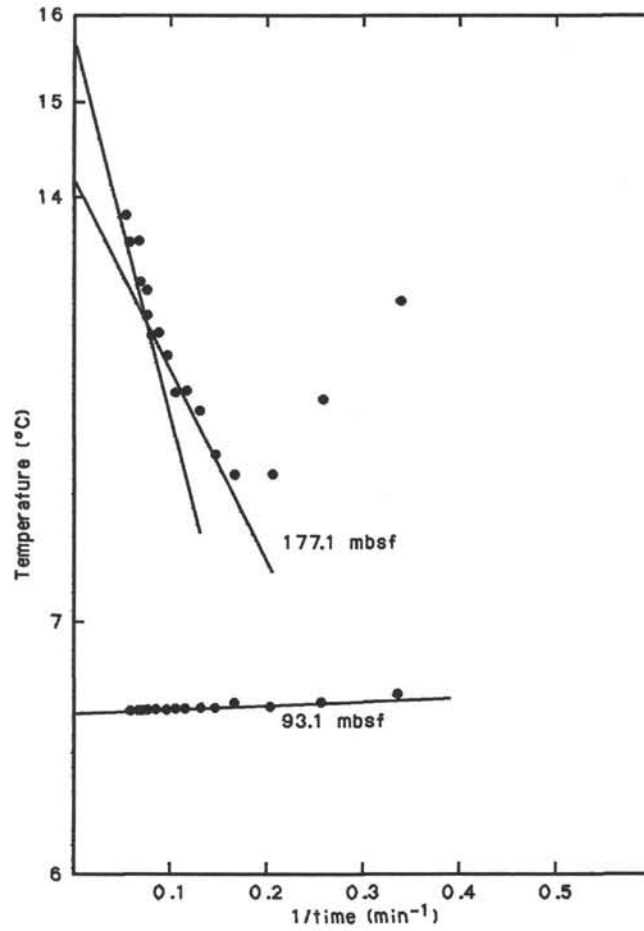


Figure 23. Graph of temperature vs. 1/time for Uyeda probe measurements at Site 745 (see Fig. 22 for initial penetration time and for temperature vs. time curves on which this figure is based).

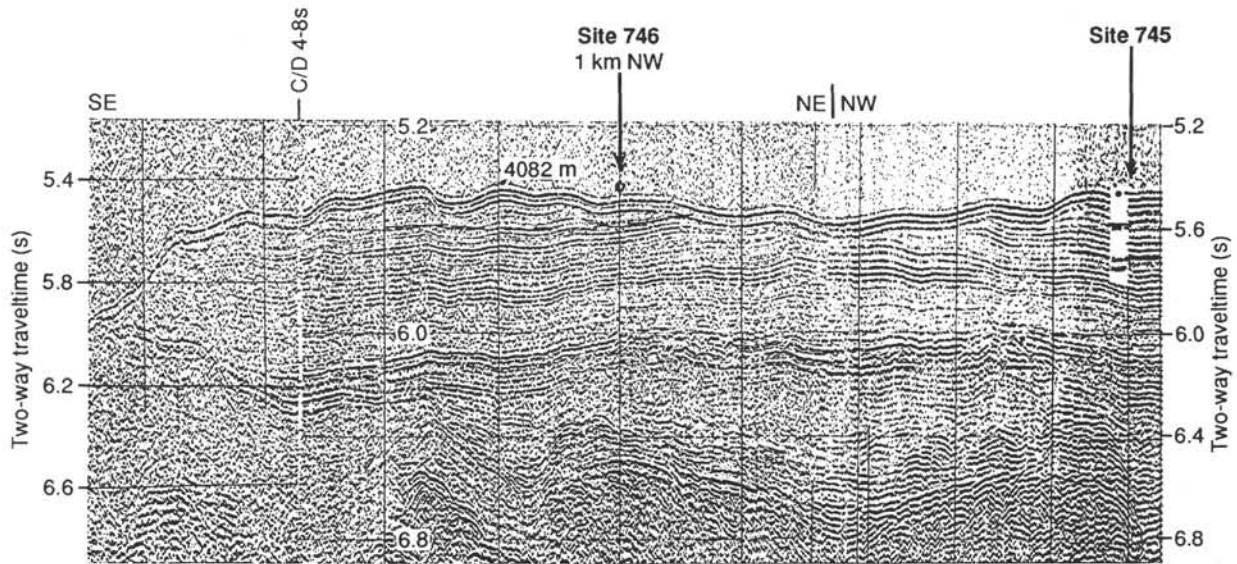


Figure 24. Seismic section (single channel) across the East Kerguelen Sedimentary Ridge and back to Site 745 (for track, see Fig. 1). Site 746 is about 1 km northwest of the indicated point. The layers deeper than the strong reflector at 6 s TWT are not discussed in the text.

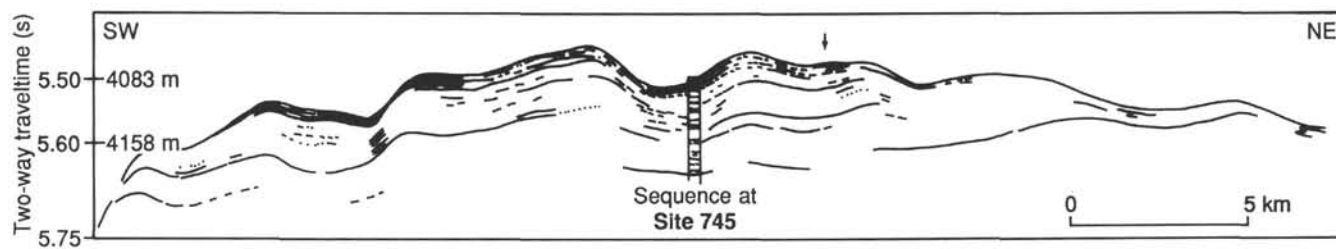


Figure 25. Sketch of seismic reflections observed on the 3.5-kHz PDR record about 2 km north of Site 745 on the top of the East Kerguelen Sedimentary Ridge. Note the wavy seafloor (arrow) and the difference in sediment thickness across the ridge. The profile is nearly  $45^\circ$  to the orientation of the sediment waves.